1. Report No.	2. Government Accession No.	3. Recipient's Catalog No.
FHWA/TX-05/0-1700-5		

4. Title and Subtitle	5. Report Date
PRELIMINARY CHARACTERIZATION OF AGGREGATE COEFFICIENT OF THERMAL EXPANSION AND GRADATION FOR PAVING CONCRETE	July 2004 Published: January 2007
	6. Performing Organization Code
7. Author(s)	8. Performing Organization Report No.
Anol K. Mukhopadhyay, Siddharth Neekhra, and Dan G. Zollinger	Report 0-1700-5
9. Performing Organization Name and Address	10. Work Unit No. (TRAIS)
Texas Transportation Institute The Texas A&M University System College Station, Texas 77843-3135	11. Contract or Grant No. Project 0-1700
12. Sponsoring Agency Name and Address	13. Type of Report and Period Covered
Texas Department of Transportation Research and Technology Implementation Office P. O. Box 5080 Austin, Texas 78763-5080	Technical Report: September 2000-March 2004
	14. Sponsoring Agency Code

15. Supplementary Notes

Project performed in cooperation with the Texas Department of Transportation and the Federal Highway Administration.
Project Title: Improving Portland Cement Concrete Pavement Performance
URL: http://tti.tamu.edu/documents/0-1700-5.pdf

16. Abstract

This report is primarily focused on measurement and modeling of aggregate coefficient of thermal expansion (COTE) and its effect on early-age crack patterns. This report also covers the aggregate gradation effects on early-age concrete properties.

A new mineralogical approach is introduced to predict the COTE of aggregate and concrete. Basically, a modeling approach is developed based on the assumption that the COTE of aggregate and concrete can be predicted from the COTE of their constituent components. Volume percentage, COTE, and elastic modulus of each constituent mineral phase are considered as inputs for the aggregate COTE model, whereas the same properties for coarse aggregate and mortar are considered for the concrete COTE model. Methods were formulated to calculate the mineral volume percentage from bulk chemical analysis for different types of rocks commonly used as aggregates in Texas. A dilatometer testing method was established to measure the COTE of aggregate and pure minerals. Calculated aggregate COTE based on the determined COTE of pure minerals and their respective calculated volume percentages show a good resemblance to the measured aggregate COTE by use of dilatometry. Similarly, predicted concrete COTE based on the calculated COTE of aggregate and mortar and their respective volume percentages compared well with the dilatometer measured concrete COTE. Such a favorable comparison between predicted and measured COTE provided a basis to establish the composite model to predict aggregate and concrete COTE.

Aggregate gradation effects on cracking-related displacements of concrete were investigated in the laboratory using the German cracking frame. Concrete workability was assessed by use of the slump and drop tests (German DIN 1048) for two different concrete mixtures consisting of gap-graded and dense-graded aggregates. Shrinkage strain, cracking frame strain, and concrete strain were measured and compared with strength gain and creep development. The measured and calculated strains of the different aggregate gradations were compared with each other. Gradation effects on strength and stress development relative to tensile cracking at the saw-cut tip were also investigated.

17. Key Words	18. Distribution Statement
Coefficient of Thermal Expansion, Concrete, Aggregate, Bond Strength, Thermal Expansion, Mineral, Dilatometer, Aggregate Gradation	No restrictions. This document is available to the public through NTIS: National Technical Information Service Springfield, Virginia 22161 http://www.ntis.gov

19. Security Classif. (of this report)	20. Security Classif. (of this page)	21. No. of Pages	22. Price
Unclassified	Unclassified	124	

PRELIMINARY CHARACTERIZATION OF AGGREGATE COEFFICIENT OF THERMAL EXPANSION AND GRADATION FOR PAVING CONCRETE

by

Anol K. Mukhopadhyay
Associate Research Scientist
Texas Transportation Institute

Siddharth Neekhra
Graduate Assistant Research
Texas Transportation Institute

and

Dan G. Zollinger
Associate Research Engineer
Texas Transportation Institute

Report 0-1700-5
Project 0-1700
Project Title: Improving Portland Cement Concrete Pavement Performance

Performed in cooperation with the
Texas Department of Transportation
and the
Federal Highway Administration

July 2004
Published: January 2007

TEXAS TRANSPORTATION INSTITUTE
The Texas A&M University System
College Station, Texas 77843-3135

DISCLAIMER

The contents of this report reflect the views of the authors, who are responsible for the facts and the accuracy of the data presented herein. The contents do not necessarily reflect the official view or policies of the Texas Department of Transportation (TxDOT) and/or the Federal Highway Administration (FHWA). This report does not constitute a standard, specification, or regulation. The engineer in charge of the project was Dan G. Zollinger, Texas P.E. #67129.

ACKNOWLEDGMENTS

The authors wish to express their appreciation to the Texas Department of Transportation personnel for their support throughout this study, as well as the Federal Highway Administration. We would also like to thank the project directors Dr. Andrew Wimsatt, Dr. Moon Won, and Mr. George Lantz and the members of the project monitoring committee.

TABLE OF CONTENTS

Page

TABLE OF CONTENTS (Continued)

Page

TABLE OF CONTENTS (Continued)

Page

TABLE OF CONTENTS (Continued)

Page

LIST OF FIGURES

LIST OF FIGURES (Continued)

Figure **Page**

LIST OF TABLES

LIST OF TABLES (Continued)

Table **Page**

CHAPTER 1. INTRODUCTION

The bulk of this report focuses on research results regarding measurement and modeling of the coefficient of thermal expansion (COTE) of aggregate materials, which can serve as a quality control measure in concrete pavement construction. This report also covers aggregate gradation effects on early-age concrete properties.

PROJECT BACKGROUND

Thermal characteristics of concrete are of interest in concrete pavement behavior and performance. Volumetrically speaking, the COTE plays a key role in the effect of thermally induced bulk strains and stresses on concrete. In continuously reinforced concrete (CRC) pavements, the continuity of the concrete is interrupted by a large number of transverse cracks, caused by volumetric changes in the concrete that result from shrinkage and temperature changes. Cracking patterns in CRC pavement are largely influenced by the COTE of the concrete and the steel reinforcement design. The COTE of concrete largely depends on the COTE of the aggregate used in the concrete mixture.

Most paving materials experience changes in volume due to changes in temperature, and this dependency is characterized in terms of COTE. Concrete is not an exception to this behavior, and the COTE of concrete depends on the thermal behavior of its individual components (i.e., coarse aggregate [CA], fine aggregate [FA], and hydrated cement paste [HCP]). The types of CA and FA and their proportions in the concrete mixture play an important role in the final COTE of the concrete (*1*). The COTE of the aggregate determines the thermal expansion of the concrete to a considerable extent because the aggregate composes about 70-75 percent of the total solid volume of the mixture. During the past decade, several researchers have shown that the thermal properties of cement mortar and aggregates can affect the thermal behavior of concrete (*2*). The COTE of the aggregate, to a large degree, affects the thermal change in concrete more strongly than the COTEs of other components in concrete as temperature changes (*3, 4*). The mechanisms associated with pavement distresses such as blowups, faulting, corner breaks, and spalling have components related to the thermal expansion properties

of concrete (*5*). Therefore, characterization of key aggregate properties should improve projection of concrete behavior with reasonable accuracy, which in turn should result in improved design and quality control and longer performing pavements. No method currently exists to measure the COTE of as-received aggregate; therefore, a test method that can measure aggregate COTE in this regard could be of use to TxDOT and other specifying agencies. Available test data indicate that COTE values vary widely among different aggregates with differing mineralogical contents and from different geographical locations. For example, some siliceous aggregates (e.g., gravel, sandstone) that consist mainly of quartz exhibit high COTE (5.56×10^{-6}/°F to 7.22×10^{-6}/°F), whereas some pure limestone aggregates that consist mainly of calcite exhibit lower COTE (3.10×10^{-6}/°F to 3.39×10^{-6}/°F) (*3, 5, 6, 7*). These results indicate that the COTE of an aggregate is mainly dependent on the COTE of the constituent minerals and their respective amounts in the aggregate. Since aggregates are composite materials consisting of different minerals in different proportions, it is assumed that aggregate properties can be determined from the properties of its component minerals (*8*). In this context, a new mineralogical aggregate COTE model is introduced. This composite model predicts aggregate COTE from the COTE of constituent minerals and their respective volume percentages. Similarly, concrete COTE can be modeled using the COTE of the constituent coarse aggregate and mortar. This composite model can be validated based on favorable comparisons between calculated and measured COTE. Accordingly, the dilatometer was used to measure the COTE of minerals, aggregates, and concrete in this context.

Another aspect of the reported research addresses aggregate gradation in concrete paving. Concrete mixture proportions typically deal with only two aggregate fractions (i.e., coarse and fine aggregates), complying with the gradation requirements stipulated in American Society of Testing and Materials (ASTM) 33. The resulting gradations are usually gap-graded (i.e., lack of gradual change in particle size) with very little intermediate material occurring between the 3/8 inch and #8 sieve sizes. A dense-graded aggregate can be made by incorporating an intermediate aggregate (e.g., pea gravel) with conventionally graded coarse and fine aggregates. Gap-graded aggregates can have a lower dry rodded unit weight (DRUW) and a larger total volume of voids to be filled with

cement mortar than concrete with dense-graded aggregates. Concrete mixtures containing gap-graded aggregates generally show higher drying shrinkage, creep, and lower strength than concrete mixtures with dense-graded aggregates. Therefore, research on formulating mixtures with dense aggregate gradation and investigating the effect of dense-graded concrete mixtures on key material properties (e.g., drying shrinkage, creep, and workability) in comparison to conventional mixtures with gap-graded aggregate would be beneficial to improve quality. The ultimate aim is to develop a better mix with relatively low shrinkage, high strength, and better workability by optimizing the aggregate gradation and reducing the cement content.

PROJECT RESEARCH OBJECTIVES

The objectives of the research project are as follows:

- Discuss the effects of aggregate properties and behavior on CRC pavement performance.
- Discuss existing methods of determining the coefficient of thermal expansion of aggregates.
- Develop an apparatus for laboratory testing of the coefficient of thermal expansion of aggregate (as-received) and concrete.
- Develop a direct composite concrete coefficient of thermal expansion model. A favorable comparison between modeled COTE and dilatometer measured COTE will be the basis to validate the models. Composite COTE modeling will serve as a check of aggregate source variability in terms of quality control and improved design and quality control measures of concrete.
- Evaluate aggregate gradation effects on concrete early-age properties.
- Evaluate the effects of aggregate blending on concrete coefficient of thermal expansion and bond strength.
- Develop designs and specifications for high-COTE aggregates.

PROJECT WORK PLAN

The project work plan consisted of two tasks related to the above objectives and is described in the following section.

Develop a Direct Concrete COTE Model

Developing a concrete COTE model was based on a two-step approach: (i) developing and validating an aggregate mineralogical COTE model and (ii) developing and validating a concrete COTE model. Following are the steps involved in developing a direct concrete COTE model:

1. Determine the COTE of two concrete specimens provided by the Materials and Pavements Division of TxDOT using the dilatometer and compare with the COTE for the same specimens obtained using the TxDOT concrete COTE method.
2. Measure the COTE for five commonly used aggregates (e.g., pure limestone, impure limestone, sandstone, granite, and gravel) commonly used across the state of Texas using the dilatometer.
3. Develop an aggregate COTE model according to the following steps:
    - Derive a mathematical equation for an aggregate COTE model based on the concept of composite modeling, where the determined COTE of pure minerals, their respective weight percentage, and their elastic modulus are required inputs.
    - Develop methods to estimate the constituent mineral weight percentages from bulk chemical analysis of each aggregate.
    - Develop a sampling protocol to obtain a representative powder sample of each aggregate (necessary for chemical analysis) and its source variability with respect to mineralogy.
    - Measure the COTE of five major minerals (quartz, albite, orthoclase, dolomite, and calcite) using the dilatometer. These five minerals constitute the expected range of mineralogy of Texas aggregates and will provide a broad-based mineralogical input for the composite COTE model.
    - Predict aggregate COTE using the derived composite model where required inputs are determined through the above steps.
    - Validate the composite model based on favorable comparisons between predicted COTE (model) and measured COTE (dilatometer).

4. Develop a concrete COTE model according to the following steps:

- Make concrete specimens (4 × 8 inch [10.2 × 20.3 cm]) using the five coarse aggregates, where the proportions of fine aggregate, coarse aggregate factor (CAF), air contents, fly ash replacement, and water to cementitious materials (w/cm) ratio remain constant.
- Measure the COTE of all concrete specimens using dilatometry.
- Measure the COTE of a standard mortar specimen using the same sand and similar sand to cement ratio that was used in the concrete by dilatometry.
- Derive a mathematical equation for the concrete COTE model based on the concept of Hirsch's composite modeling (*8*) where the determined COTE of mortar and coarse aggregates, their respective weight percentage, and their elastic modulus serve as inputs.
- Calculate the concrete COTE from the derived composite model.
- Compare the calculated COTE from the model with the measured COTE. A favorable comparison with high correlation coefficient (R^2) will validate the concrete composite model.

Aggregate Gradation Effects Related to Concrete Spalling and Cracking

Evaluate the effects of aggregate gradation on the potential for concrete spalling and cracking relative to the following:

- compressive, tensile, and fracture strengths versus time;
- concrete shrinkage and concrete relative humidity levels;
- concrete creep over time; and
- concrete workability in terms of slump, harshness, and mobility (mobility and harshness will be assessed using the German drop test [DIN 1048] and a standard ASTM slump cone).

Use the testing data to relate the strength of the concrete and the stress levels associated with spall-related delamination and crack pattern development in CRC pavement construction in terms of curing, aggregate gradation, mixture design, and crack control to delimit favorable combinations of each.

CHAPTER 2. LITERATURE REVIEW OF AGGREGATE COTE EFFECTS ON CRC PAVEMENT PERFORMANCE

REVIEW OF DIFFERENT COARSE AGGREGATE EFFECTS ON CRC PAVEMENT PERFORMANCE

Concrete is a heterogeneous mixture of cement, water, fine aggregates, and coarse aggregates. Coarse aggregates normally constitute about 75 percent of the volume of concrete and therefore have a major influence on the properties of concrete. The coefficient of thermal expansion of concrete is one such property that is mainly controlled by the type and amount of coarse aggregate. In the next section some properties of aggregates are described along with a detailed explanation of the COTE of aggregate and its effects on concrete.

The roles of physical, mechanical, and chemical properties of coarse aggregates on the behavior and performance of paving concrete (*9*) are often described in terms of their effects on concrete strength, shrinkage, creep, and bond strength. Specific aggregate properties are listed in Table 1 relative to their physical attributes.

Table 1. Aggregate Properties.

Physical	Mechanical	Chemical
Particle shape	Strength	Solubility
Maximum particle size	Elastic modulus	Base exchange
Surface texture	Coefficient of thermal expansion	Surface charge
Percent voids	Resistance to loads	Chloride content
Thermal conductivity	Resistance to degradation	Reactivity
Permeability		Slaking
Specific gravity		Coatings
Porosity		Oxidation potential
Gradation		Resistivity

These physical attributes relate to concrete mixing, placing, finishing, hardening, and other construction and pavement related characteristics. The mechanical properties

of an aggregate predict its ability to resist loads and stresses, hardened concrete behavior. The chemical properties of an aggregate are a result of its chemical composition and are related to how the aggregate chemically interacts with concrete pore solution and water. COTE could be classified as a mechanical property of aggregate. A previously suggested classification procedure derived from aggregate properties is illustrated in Figure 1.

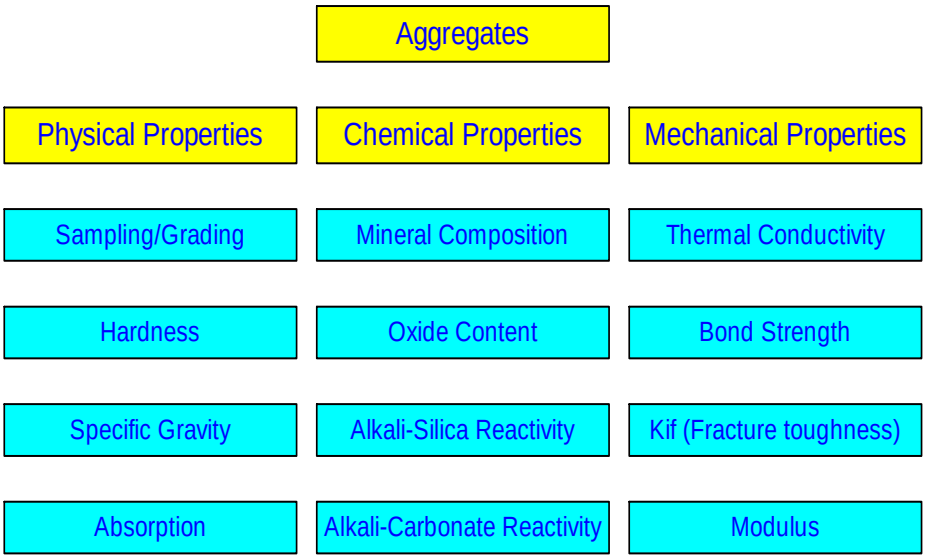

Figure 1. Aggregate Classification (*10*).

In discussion of the many aggregate related aspects of concrete performance in a CRC pavement system it is useful to suggest minimum criteria for aggregate classification including indicators of aggregate hardness, coefficient of thermal expansion, and shape and texture.

Coarse aggregate constitutes a major part of portland cement concrete and is therefore a major determinant of its performance. A classification system for coarse aggregate would provide a systematic means for identification of aggregates, which could be used in the selection of aggregates for different design and construction combinations.

The ultimate goal of such a classification scheme is to optimize the selection of coarse aggregate to be used in construction of concrete pavements. The backbone of a system to classify coarse aggregates is based on keying on a few significant properties of coarse aggregates which affect performance. Properties related to hardness, COTE, and

shape and texture along with methods to measure these properties are described below in detail.

Hardness

The ability of aggregate to resist the damaging effect of abrasive forces under loads applied to a pavement surface or through handling in transportation or mixing cycles is measured as hardness but relates to the abrasion resistance of the aggregate. The aggregate must resist the abrasive action that may otherwise lead to degradation and disintegration when stockpiled, mixed, placed, compacted, or exposed to loading forces. Hardness is also an indicator of the types of minerals present in the aggregate source.

Measurement of Aggregate Hardness

The Scratch Hardness test is used to determine the relative hardness of two materials. The Scratch Hardness test is based on the Mohs hardness test (Table 2), where the hardness of one material is known and is used as a reference to determine the hardness of the unknown material based on the capability of the known material to scratch the unknown material. Different levels of hardness are referenced to a series of 10 minerals, which are ranked in order of increasing hardness from 1 to 10 (Table 2). A mineral that will scratch another has a higher Mohs hardness number than the mineral that was scratched.

Table 2. Mohs Scale of Hardness.

Mohs Number	Mineral	Mohs Number	Mineral
1	Talc	6	Orthoclase (Feldspar)
2	Gypsum	7	Quartz
3	Calcite	8	Topaz
4	Fluorite	9	Corundum (or Sapphire)
5	Apatite	10	Diamond

Mohs scale of hardness is designed to identify unknown minerals based on their relative scratched hardness with respect to the known hardness of 10 minerals. The same approach can be applied to categorize aggregate based on their relative scratched hardness in a broader spectrum. Table 3 categorizes types of aggregate based on

scratched hardness. The scratched hardness may also be determined as a function of the type of minerals and their percentages in the aggregate. A weighted average of the scratched hardness of the minerals present in an aggregate can be representative of the hardness of that aggregate.

Table 3. Scratch Hardness as a Function of Aggregate Type and Mineralogy.

Aggregate	Major Constituent Mineral(s)	Scratched Hardness Range
Pure limestone (LST)	Calcite	~ 3
Impure limestone	Calcite, quartz, dolomite, feldspar	~ 3 if the total impurities do not exceed 10%; > 3 if the total impurities exceed 10%. Hardness of quartz and feldspar is around 6-7.
Siliceous river gravel (SRG)	Mainly silica minerals, e.g., quartz, chalcedony, opal, etc.	~ 7
Heterogeneous gravel	Siliceous rock (e.g., quartzite, chert) along with igneous rock (e.g., granite, basalt) and sedimentary rock (e.g., sandstone)	Hardness varies (5-7) depending upon relative proportion of different rock. Weighted average could be a better average estimation.
Calcareous gravel	Mixture of limestone and siliceous rock (quartzite, chert)	Depending on relative proportion of different rock, e.g., 4-5 if 50:50 (calcareous:siliceous), 3-4 if 90:10.
Granite (GRN)	Quartz, feldspar, mica, amphibole, apatite	~ 6 but it could vary from 5-7
Sandstone (SST)	Quartz, feldspar, calcite, iron oxides, rock fragments	Quartz dominated (e.g., ortho-quartzite) ~7 Both quartz and feldspar (e.g., arenite) 6-7

Coefficient of Thermal Expansion

COTE of aggregate is one of the most important behavioral characteristics of an aggregate material, which is found to influence the performance of concrete pavement primarily due to its effect on dimensional change under a change in temperature. COTE of aggregate has a marked effect on the COTE of concrete containing the given

aggregate. Some pavement distresses such as blowups, faulting, corner breaks, and spalling are related to the thermal expansion properties of jointed concrete (*5*), but the more pronounced effect is on the development of the crack pattern and the daily and seasonal temperature changes on the width of transverse cracks in CRC pavements, as it would affect their load transfer efficiency. Knowledge of this property during the design stage allows accurate prediction of the potential thermal change on crack development and crack width and enhances the overall design process. Authors of this study suggest that aggregate COTE can be divided into three categories (Table 4) based on their effects on concrete performance.

Table 4. COTE Based Aggregate Categories.

Category	COTE (10^{-6}/°F)
Low	< 3.5
Medium	3.5-5.0
High	> 5.0

Aggregate Shape and Texture

The shape and texture of the aggregates in concrete play a very important and crucial part in the development of the short-term strength of the concrete during early hydration stages and on workability properties while in a fresh state. Specifically, the mechanical strength of the aggregate bond depends on aggregate texture. Excessive smoothness may hamper formation of a mechanical bond between the aggregate and the cement paste at an early age. Factors affecting bond strength are the degree of mechanical interlock, available surface area for bonding, and shape of the aggregates. Smooth particles not only lack mechanical interlock but also maintain a lower bonding area between the aggregate surface and the binder.

Particle shape and texture also affect the workability and the ability to place and consolidate concrete in a fresh state. Equi-dimensional particles produce higher density and higher strength concrete, whereas flat and elongated particles pack poorly with the binder and decrease workability (*11*, *12*). Flakiness of coarse aggregates affects workability and mobility of concrete, which ultimately increases water demand. Increased water demand affects fresh concrete properties by causing bleeding and

segregation. Ultimately, these adverse affects may cause reduction in strength and performance of concrete.

Measurement of Aggregate Shape and Texture

Aggregate shape and texture characteristics can be analyzed using the Aggregate Imaging System (AIMS). AIMS has the ability to analyze the angularity and texture of fine and coarse aggregates. Figure 2 shows a conceptual three-dimensional (3-D) graphical model of AIMS illustrating the various components of the system, and Figure 3 shows a picture of the entire AIMS setup. AIMS utilizes three closed-loop direct-current (DC) servo motor linear actuators with 9.84 inch (250 mm) of travel along the x- and y-axes and 2 inch (50 mm) of travel along the z-axis. Travel along three axes allows for precision movement in all three directions simultaneously and independently. The x-axis motion runs on a slider bar where the camera is attached. The y-axis motion of the aggregate tray and backlighting table runs on a bearing guide assembly, which creates smooth, uniform motion. The z-axis controls the auto-focusing of the camera. The autofocus utilizes high spatial frequency for a signal of a video microscope connected to the camera.

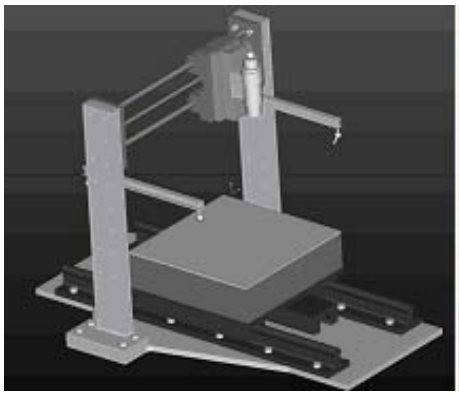

Figure 2. 3-D Graphical Model of AIMS.

Figure 3. The AIMS System.

The video microscope has a 16:1 zoom ratio, allowing capture of a wide range of particle sizes without changing parts. A black and white video camera with external controls is used. The camera is connected to a magnification lens. The camera and video

microscope are attached to a dovetail slide with a motion range of 11.81 inch (300 mm) along the z-axis in order to capture images over a wide range of aggregate sizes. All motions connect to a multi-axis external controller that offers both manual and automatic control of motion, as well as enhanced black level and contrast controls. The system operates based on two modules. The first module is for the analysis of fine aggregates (smaller than 0.187 inch [4.75 mm]), while the second is devoted to the analysis of coarse aggregates. The system is capable of analyzing the three dimensions of aggregates. It also uses two different image analysis techniques to quantify the irregularity of a particle surface, or angularity. Wavelet analysis is used to measure the different scales or levels of texture present on a particle surface (*11*).

The AIMS software sorts the three dimensions and calculates sphericity as shown in equation (1):

$$\text{Sphericity} = \sqrt[3]{\frac{d_s . d_I}{d_L^2}} \quad (1)$$

where d_L is the longest dimension, d_I is the intermediate dimension, and d_s is the shortest dimension. These are the dimensions measured while analyzing the image using AIMS. Aggregate form is characterized in four categories based on sphericity index as shown in Table 5.

Table 5. Categories of Sphericity.

Category	Sphericity Index
Flat/Elongated	< 0.5
Low sphericity	0.5-0.6
Moderate sphericity	0.6-0.8
High sphericity	> 0.8

Texture index is the arithmetic mean of the detail coefficients at that level for the three images (horizontal direction, vertical direction, and diagonal direction). Mathematically,

$$Texture\ Index_n = \frac{1}{3N}\sum_{i=1}^{3}\sum_{j=1}^{N}\left(D_{i,j}(x,y)\right)^2 \quad (2)$$

where N denotes the level of decomposition, *i* takes values 1, 2, or 3, for the three detailed images of texture, and *j* is the wavelet coefficient index $D_{n,i}(x,y)$. These values are determined using wavelet analysis. Aggregate texture is categorized in five categories based on texture index as shown in Table 6.

Aggregate effects on the behavior of concrete are described in terms of:

- *abrasion resistance* - hardness;
- *alkali-aggregate reaction* - presence of particular siliceous constituents;
- *strength* - strength, surface texture, cleanness, particle shape, and maximum size;
- *shrinkage and creep* - modulus of elasticity, particle shape, grading, cleanness, maximum size, and clay minerals;
- *unit weight* - specific gravity, particle shape, grading, and maximum size; and
- *modulus of elasticity* - creep, Poisson's ratio, and volumetric deformation.

Table 6. Aggregate Texture Categories.

Category	Texture Index
Polished	< 200
Smooth	200-350
Low roughness	350-550
Moderate roughness	550-750
High roughness	> 750

Performance-wise, delamination/spalling (Figure 4), punchout, and widened transverse cracks are common distresses seen in CRC pavements. Combined effects of key aggregate and non-aggregate related factors (e.g., ratio of steel bond area to concrete volume, depth of steel cover, sub-base friction characteristics, slab thickness, etc.) are related to these distresses.

Figure 4. Spalling in CRC Pavement *(13)*.

Previous field studies (*14, 15*) have confirmed that spalling distress is a consequence of delaminations that formed at an early pavement age resulting primarily from shearing action induced by large moisture gradients induced by the method of curing. The moisture gradient develops because of evaporation and differential drying shrinkage, which is a function of ambient temperature and curing conditions during and after concrete placement (Figure 5). Typically, delamination is relatively shallow (Figure 6) and occurs at an early concrete age when the stresses caused by moisture variation surpass the shear strength of the concrete. Significant spalling is not likely to occur where delaminations are non-existent. Conditions necessary for delamination formation include low interfacial strength between the aggregate and mortar and sufficient evaporation that results in differential drying shrinkage near the pavement surface. Temperature variation may be a factor in the development of delamination shear fractures but is presumed to contribute considerably less than shrinkage does. Once delaminations form, they may later extend into spalls as a result of incompressibles, freeze-thaw cycles, traffic loading, and other similar effects.

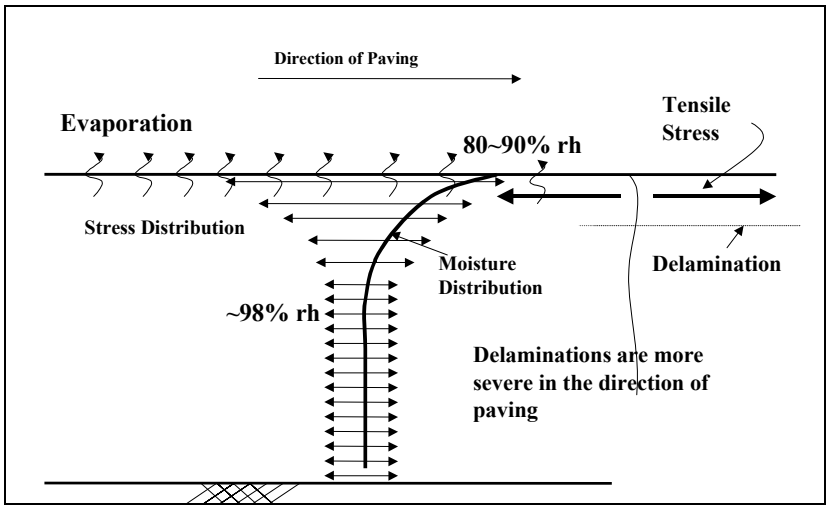

Figure 5. Moisture and Shrinkage Gradients Leading to Delamination (*13*). rh = relative humidity.

As described above, aggregate properties play a very important role in the performance of CRC pavements. In a CRC pavement the key element to developing a

uniform crack pattern is maintaining a balance between the following aggregate factors that affect pavement performance, listed in order of importance:

- concrete aggregate/paste early-age bond strength;
- concrete drying shrinkage and creep;
- aggregate type, gradation, and blend effects;
- aggregate coefficient of thermal expansion;
- concrete strength; and
- modulus of elasticity.

Figure 6. Delamination of Unspalled Core (*13*).

The present study focuses on the role of aggregate COTE and aggregate gradation on early-age concrete properties, which are described in detail below.

Role of Aggregate COTE on CRC Pavement Performance

COTE is a key material property that characterizes the change in material volume with a change in temperature. COTE is actually a length change in a unit of length per degree temperature change. The coarse aggregate is expected to have the dominant effect upon the thermal expansion behavior of concrete, as previously discussed. Several researchers have determined the COTE of various aggregates, and their results indicate that COTE varies widely among different aggregates with respect to mineralogical

variation and geographic location. Siliceous aggregates such as chert, quartzite, and sandstone exhibit higher COTE values (e.g., 5.56×10^{-6}/°F to 6.67×10^{-6} /°F), whereas limestone aggregates exhibit lower COTE values (e.g., 2.78×10^{-6}/°F to 3.89×10^{-6}/°F) (*3, 5, 6, 7*). The COTE of basalt, granite, and gneiss generally vary between 3.33×10^{-6}/°F and 5.0×10^{-6}/°F. The data have also demonstrated that aggregates of the same type and from the same source may vary significantly in COTE values. Therefore, COTE characterization of an assorted mixture of aggregates needs improvement in order to better understand the behavior patterns of concrete structures and concrete pavements made with different types of aggregates. The researchers anticipate that an estimated value of the COTE for concrete may be calculated from the weighted averages of the COTE of the aggregates and the hardened cement paste. Therefore, mix proportion of concrete is a vital consideration to estimate concrete COTE. However, the two main constituents (i.e., cement paste and aggregate) have dissimilar COTE values. Cement paste properties depend mainly on the water content for a given type of cement. Mitchell and Meyers (*2, 3*) showed that variations in moisture content cause the COTE to vary significantly. Minimum COTE values were measured in oven-dried and saturated cement, while maximum values were obtained at intermediate moisture contents of about 65 to 70 percent for ages up to six months. R.E. Davis (*6*) researched factors that influence the magnitude of thermal volume changes in mortar and concrete. He found that COTE increases with an increase in the richness of the mix. He also found that the brand of cement influences thermal expansion. Initially, COTE increases with age for a short period and then levels off to a constant value. Cement paste can have COTE values from less than 5.0×10^{-6}/°F to as much as 11.67×10^{-6}/°F, depending on the water to cementitious ratio, moisture content, and cement fineness and composition.

The two main constituents of concrete relative to concrete thermal behavior (i.e., mortar and coarse aggregate) combine to form a composite coefficient of thermal expansion of concrete. Since more than half of the concrete volume is coarse aggregate, the major factor influencing the COTE of concrete is the COTE of coarse aggregate. Studies conducted by Brown (*16*) and later by Won et al. (*17*) showed that the effect of silica content in the aggregate on the COTE of the concrete is significant. These studies indicate the higher the silica content, the higher the COTE of the concrete. The COTE of

concrete certainly plays a role in the thermal induced opening and closing of transverse cracks in CRC pavements. Thermal effects are manifested in the daily variation in the opening and closing of transverse cracks. This opening and closing contributes to stress in the reinforcing steel, but only to the extent that the COTE of the steel reinforcement is greater than the COTE of the concrete. Consequently, the effect due to temperature on steel stress is often much lower than the effect due to drying shrinkage. However, the opening and closing of cracks is a factor in performance, since the degree of load transfer is directly related to the width of the cracks. Therefore, crack widths should be restricted within certain limits. Typically, the design steel percentage is based on the stress in the steel at mature concrete ages, but past performance studies clearly indicate that more emphasis should be placed on crack width of the transverse cracks and its effect on load behavior over the design life. The thermal behavior of the coarse aggregate may play a greater role in the opening and closing of cracks after creep effects of concrete are diminished due to aging and maturing of the concrete.

Aggregate Type, Gradation, and Blend Factors on CRC Pavement Performance

Pavement performance varies with the type of aggregate used. Present aggregate selection criteria may not take into account all of the aggregate properties that affect performance. Bond strength, reactivity, and the expansion properties of an aggregate are related to performance.

TxDOT Projects 0-1244 and 7-3925 investigated material properties of crushed limestone and siliceous river gravel to determine the relationship between the properties of single-aggregate concretes and concrete made with predetermined blends of limestone and gravel by keeping the mixture parameters constant while varying the coarse aggregates used. The results from the test program indicated that equal performance could be obtained from aggregates of widely varying properties; however, the effects of high-COTE aggregates need to be offset by mixture design and the use of blended materials or even by construction procedures. Although the crushed-limestone concrete had higher compressive and tensile strengths than the river gravel concrete, the crushed-limestone concrete did not provide higher load transfer efficiency. This discrepancy may be due to different behaviors of limestone and river gravel in concrete fracturing. With

intermediate aggregate in concrete, aggregate interlocking would be improved and, therefore, load transfer performance at the joint would improve.

Effect of Aggregate Gradation

Present TxDOT specifications call for a gap-graded aggregate gradation for paving concrete mixes that includes higher mortar (paste + sand) content. In conventional concrete mixtures with gap-graded aggregate gradation, a deficiency of particles between the 3/8 inch (9.53 mm) and #8 sieve (0.092 inch [2.36 mm]) necessitates greater amounts of mortar. Use of a low-mortar concrete may have minimal effect on direct placement costs while facilitating ease of placement and finishability. The aggregate fraction in concrete can play a role in filling voids to provide the mobility needed for placement and finishing. The above-mentioned deficiency in gap-graded aggregate gradation can be compensated by adding particles of intermediate size (between 3/8 inch and the #8 sieve) to get a combined gradation with uniform and gradual particle size distribution that, if rounded, ensures best voids filling and low water demand. Particle distribution can be observed by plotting combined aggregate gradation on the 0.45 power chart. For a mix containing well-graded aggregate, the trend line should be as linear as possible. On the other hand, the gradation trend for concrete containing gap-graded aggregate generally falls off the 0.45 power chart straight line.

The shape of particles ranging from 0.185 inch (4.75 mm) to 0.092 inch (2.36 mm) in size has a major effect on workability. Rounded pea gravel or cubically crushed stone is a desirable component of concrete because it improves workability, pumpability, and finishability of the mixture along with the additional benefit of providing high strength and low shrinkage properties. On the other hand, sharp and flat-shaped particles of this size range cause mix mobility problems (i.e., poor workability). Experience with these mixtures has mainly utilized smooth, rounded pea gravel as the intermediate aggregate. For this reason, a crushed intermediate material may not function well. Therefore, complete understanding of optimization needs to include consideration of shape and texture of the intermediate aggregate – particularly in light of the limited sources of pea gravel and how these parameters affect the cracking behavior of a mixture in CRC pavement construction.

Effects of Aggregate Gradation on Key Material Properties

An optimum aggregate-graded mix with low slump will have better mobility than a high slump mix with conventional gap-graded aggregate. Therefore, it is possible to reduce water to cementitious ratio and increase flowability/mobility by introducing well-graded combined aggregate into the moisture. Amount of smooth, rounded intermediate aggregate plays an important role in concrete mobility. The normal slump test measures the consistency of a concrete mixture. However, consistency measured in this manner is not the best measure of workability. A German drop test method (designed to reflect concrete mobility) provides an improved measure of consistency.

As previously noted, gap-graded aggregates have a lower dry rodded unit weight and larger total volume of voids to be filled with mortar than concrete with dense-graded aggregates. Intermediate aggregate (IA) fills the major voids between the larger aggregates, reduces the need for fine particles, and increases concrete density. At the same time IA also reduces the cement content in comparison with the gap-graded aggregate mix. Theoretically, the strength of dense-graded concrete should be higher than that of gap-graded concrete. Because of the higher mortar content (cement + water + sand) in the mixture, the concrete with gap-graded aggregates may also undergo larger volumetric strain due to shrinkage. Higher water demand that is often associated with gap-graded aggregate also contributes to higher volumetric strain than concrete with dense-graded aggregate. Therefore, the benefits of dense-graded concrete should be increased strength and reduction in shrinkage stress, which should minimize undesirable crack formation, particularly for certain types of aggregate. It may be desirable to optimize a mixture by adjusting the shrinkage, creep, workability, and cost by adjustment of the aggregate gradation that affects the early-age shrinkage and cracking performance.

Optimization of a concrete mixture using gravel as a coarse aggregate will be different than for a mixture using a limestone coarse aggregate. Lowering drying shrinkage in a limestone paving mixture may not be as beneficial as it would be in a gravel mixture because of its greater propensity to crack. The goals of optimization should not automatically be lowest shrinkage and highest strength but rather whatever is needed to ensure improved performance. For CRC pavements, optimum performance means achieving optimum crack spacing (which is in the range of 6 feet [5.5 m]),

optimum crack width (less than 40 mils), and eliminating delamination and spalling. Gravel mixtures tend to underachieve these cracking parameters, and limestone mixtures may tend to overachieve them.

CHEMICAL AND MINERALOGICAL ASPECTS OF AGGREGATE COTE

Although not expressly stated, hardened concrete has a COTE greater than that of aggregate, but the expansion of concrete is proportional to that of the aggregate, as aggregates form a major part of the concrete (*5*). Aggregates commonly used in concrete are classified into three major categories: igneous, sedimentary, and metamorphic rocks. These groups can be further divided into subgroups depending on their chemical and mineral composition and their textural and internal structure. Research suggests that a definable relationship exists between the chemical and mineral composition of the aggregate and its measured COTE. In order to develop this relationship to the implementation stage, a better understanding of the mineralogical composition in relation to the chemical oxide composition of aggregate is warranted. Accurate knowledge of an aggregate's mineral composition is the key to predicting thermal change resulting from a change in temperature.

Igneous rocks are the result of solidification of molten material that originated in the Earth's interior. Magma that flows out onto the Earth's surface and cools rapidly forms volcanic rocks such as basalt, rhyolite, andesite, etc. Those that do not reach the surface and solidify slowly in the subsurface form plutonic rocks (e.g., granite, diorite, gabbro, ultrabasic rocks, etc.). Igneous rocks can be divided into three groups based on chemical composition: acidic, intermediate, and basic. Rocks rich in SiO_2 are termed acidic, and those less rich in SiO_2 are termed basic. Acidic rocks contain sufficient silica for the mineral quartz to be present. Basic rocks, on the other hand, do not have sufficient silica to form quartz. Less silica is found in feldspars, which contain other cations: Al, Na, K, and Ca. Other elements, Mg and Fe in particular, are components of olivines, pyroxenes, and amphiboles. Certain minerals are frequently found together: for example, olivine, pyroxene, and calcium plagioclase (anorthite). Others such as quartz and olivine never appear together. There exists an approximate inverse correlation between the temperature at which a mineral crystallizes from magma and its relative

resistance to alteration processes that affect all igneous rocks. Olivine and pyroxene, for example, are minerals formed at high temperatures and are easily altered. At the other extreme, quartz resists most alteration processes.

Most common sedimentary rocks are formed by weathering of pre-existing rocks (sedimentary, igneous, and metamorphic), transport of weathered products by such means as wind and moving water, deposition of suspended materials from air or water, compaction, and diagenesis. Sedimentary rocks are also formed through chemical processes such as dissolution and precipitation of minerals in water and secretion of dissolved minerals through organic agents.

Metamorphic rocks are formed by a process called metamorphism (i.e., during burial or heating, where rocks experience recrystallization and mutual reaction of constituent minerals as their stability fields are exceeded). Because these reactions take place at temperatures below the silica melt phase, they are called metamorphic. After formation, most rocks are exposed to a series of processes and cannot be classified by a single process.

The variation of the COTEs of the different types of aggregates can be explained by the presence and proportions of the different types of minerals they contain. It is true that different rock types commonly used as aggregates have characteristic chemical compositions. Therefore, differences in chemical composition should ultimately reflect different mineralogies. The chemical composition changes if the rock type changes. Aggregate from the same source could have slightly different COTE values because of slight variations in mineralogy or textural features like recrystallization, crystallinity, etc.

SUMMARY

Pavement performance varies with the type of aggregate used. Present aggregate selection criteria may not take into account all of the aggregate properties that affect performance. It is useful to incorporate an aggregate performance-based classification system based on selective physical (e.g., COTE, shape/texture, hardness, etc.) and chemical (e.g., alkali-silica reactivity, mineralogy, etc.) aggregate properties. Such a classification scheme will facilitate optimization of the selection of coarse aggregate to be used in construction of concrete pavements.

The common distress types in CRC pavements (e.g., delamination/spalling, punchout, and widened transverse cracks) are related to key aggregate properties (e.g., aggregate-paste early-age bond strength, aggregate type, gradation, blend effects, CoTE, etc.). Conditions necessary for delamination formation include low interfacial strength between the aggregate and mortar and sufficient evaporation that results in differential drying shrinkage near the pavement surface. Temperature variation may be a factor in the development of delamination shear fractures but is presumed to contribute considerably less than shrinkage does. Optimum performance of CRC pavements means achieving optimum crack spacing (in the range of 6 feet), optimum crack width (less than 40 mils), and eliminating delamination and spalling. The present study focuses on the role of aggregate COTE and aggregate gradation on early-age concrete properties.

- COTE of concrete certainly plays a role in the thermal-induced opening and closing of transverse cracks in CRC pavements. Knowledge of this property during the design stage allows for accurate prediction of the potential thermal change on crack development and crack width and enhances the overall design process. The two main constituents of concrete relative to concrete thermal behavior (i.e., paste and aggregate) combine to form a composite coefficient of thermal expansion of concrete. The two main constituents (i.e., cement paste and aggregate) have dissimilar COTE values. Variations in moisture content cause the COTE to vary significantly. Since more than half of the concrete volume is coarse aggregate, the major factor influencing the COTE of concrete is the COTE of coarse aggregate. The common way to offset the effects of high-COTE aggregates is to use blended aggregates.
- COTE varies widely among different aggregates with respect to mineralogical variation and geographic location. The variation of the COTE of the different types of aggregates can be explained by the presence and proportions of different types of minerals they contain. Therefore, different rock types commonly used as aggregates have characteristic chemical compositions. The mineral types and contents of an aggregate can be predicted based on the relationship between the mineralogical composition and chemical oxide composition of that aggregate.

- The benefits of concrete with optimum aggregate gradation (dense-graded) should be an increased amount of strength and a reduction in shrinkage stress, which should minimize undesirable crack formation, particularly for certain types of aggregate.

CHAPTER 3. METHODS OF TESTING FOR AGGREGATE COTE

PREVIOUS METHODS

Researchers have determined the COTE of various aggregates by applying different techniques. However, a user friendly technique or device to measure bulk as-received aggregate COTE is not in existence. The thermal expansion of the heterogeneous mixture aggregates needs to be characterized in order to better understand the behavior patterns of concrete structures and concrete pavements made with these different types of aggregates.

Many attempts have been made to measure the COTE of aggregates and concrete. Researchers have tried different methods to measure either the linear expansion (e.g., strain gage) or the volume expansion (e.g., dilatometer). Following is the list of test methods obtained from the literature survey:

1. test method to measure volume expansion of aggregate core (1 × 2 inch [2.5 × 5 cm]) specimens, explained by Willis and DeReus (*18*);
2. strain gage test method – coarse aggregate (*19*, *20*, *21*);
3. dilatometer – aggregate volume expansion (*22*, *23*); and
4. American Association of State Highway and Transportation Officials (AASHTO) TP 60-00 – linear expansion of hydraulic cement concrete (*24*).

The above-mentioned test methods (except the dilatometer) need either cylindrical specimens or specimens of other dimensions and measure expansion over a temperature range. However, these methods are not suitable to determine the COTE of fine aggregate because of the smaller size of the particles.

The method explained by Willis and DeReus (*18*) allows measurements to be made over a considerable particle size range using an optical lever. Their specimens were 1 inch (25.4 mm) diameter cores, 2 inch (50 mm) long, drilled from an aggregate specimen to be tested and placed in a controlled-temperature oil bath with a range of 37° ± 3.06°F to 140° ± 5.0°F. When the possible errors involved in the measurements are considered, the calculated COTE are probably accurate to $\pm 2 \times 10^{-6}$/°F.

Strain Gage Method

In the strain gage test method, developed by the U.S. Army Corps of Engineers (*19*), electrical resistance wire strain gages measure the COTE of a coarse aggregate. The apparatus consists of (i) a controlled-temperature cabinet, (ii) an SR-4 strain indicator, (iii) resistance electrical strain gages, (iv) suitable cement for attaching the gages to the specimens, (v) a multipoint recording potentiometer, (vi) a standard specimen of known COTE, (vii) a switchboard with silver-contact switches in circuit with the SR-4 indicator, (viii) individual lead wires to the panel board, (ix) a panel board built for mounting specimens with gages attached through binding posts to the lead wires, (x) thermocouples for temperature measurements within a cabinet at various points, and (xi) a diamond cutoff wheel for sawing specimens. Strain is measured in three mutually perpendicular directions in the specimen. Specimens of coarse aggregate are selected in a size that permits preparation of surfaces for SR-4 strain gage mounting. The SR-4 strain gages are attached using only enough cement to completely coat the gage and specimen surfaces to be joined. After a curing period, the specimens are mounted on the panel board along with the standard sample. The temperature is set to 135°F (57.2°C) and is maintained until equilibrium is reached. After equilibrium, each gage, including the standard gage, is read. The temperature setting is then changed to 35°F (1.67°C), and as soon as possible after equilibrium is attained, readings are taken again. This procedure is repeated for at least 10 cycles. The reading from the first cycle is discarded. The calculation is as follows:

$$C = 4.3\ \Delta t - (\Delta y + \Delta x) / \Delta t \qquad (3)$$

where,

C = linear coefficient of thermal expansion,

4.3 = linear coefficient of thermal expansion of quartz (10^{-6}/°F),

Δt = temperature difference between successive readings (°F),

Δy = difference between successive readings of standard gage (10^{-6} inch/inch), and

Δx = difference between successive readings of test gage (10^{-6} inch/inch).

Venecanin (*20*) reported a similar but more elaborate setup, where strain gages were mounted to obtain measurements parallel to the edges and in both diagonal directions on each of six faces of a cube of rock.

Mitchell (*21*) described a method in which specimens of 25.4 mm (1 inch) to 76.2 mm (3 inches) in size were coated with wax and held in fulcrum-type extensometer frames. The specimens were kept immersed in a circulating ethylene glycol solution held at a desired temperature, and electromagnetic strain gages with electronic indicators were used for measurement.

The main drawback of using strain gages is that they cannot be used on material of different sizes and shapes. Creep of gages cemented to the surfaces can occur during the test and cause errors in gage readings. Because of the size and usually heterogeneous nature of fine aggregate, none of the preceding methods are readily adaptable to determination of the COTE of this type of material. The usual approach has been to determine the linear expansion of mortar bars containing the fine aggregate. However, the results obtained include the effects of the length change contributed by the cement.

Dilatometer Method

The dilatometer method was devised in 1951 by Verbeck and Haas to measure the coefficient of volumetric thermal expansion of aggregate (*22*). Their apparatus (Figure 7) consisted of a 1 L (0.0353 ft^3) dilatometer flask to which was attached a laboratory-constructed capillary bulb arrangement containing electrical contacts. In operation, the flask was filled with aggregate, and water and the apparatus were allowed to equilibrate at one of the controlling electric contacts. The equilibrium temperature was measured with a Beckman thermometer. Verbeck and Haas calculated the COTE on the basis of the temperature required to produce an expansion equivalent to the volume between the equilibrating electrical contacts. The apparatus needed to be calibrated to determine the coefficient of volumetric thermal expansion of the flask. The aggregate sample was immersed in water for a few days in order to remove any air present. The temperature increment was approximately 4°C (39.2°F); however, this varied depending on the temperature at which the flask was operated, the ratio of the volume increment between the contacts to the flask volume, the amount of aggregate in the flask, and the thermal

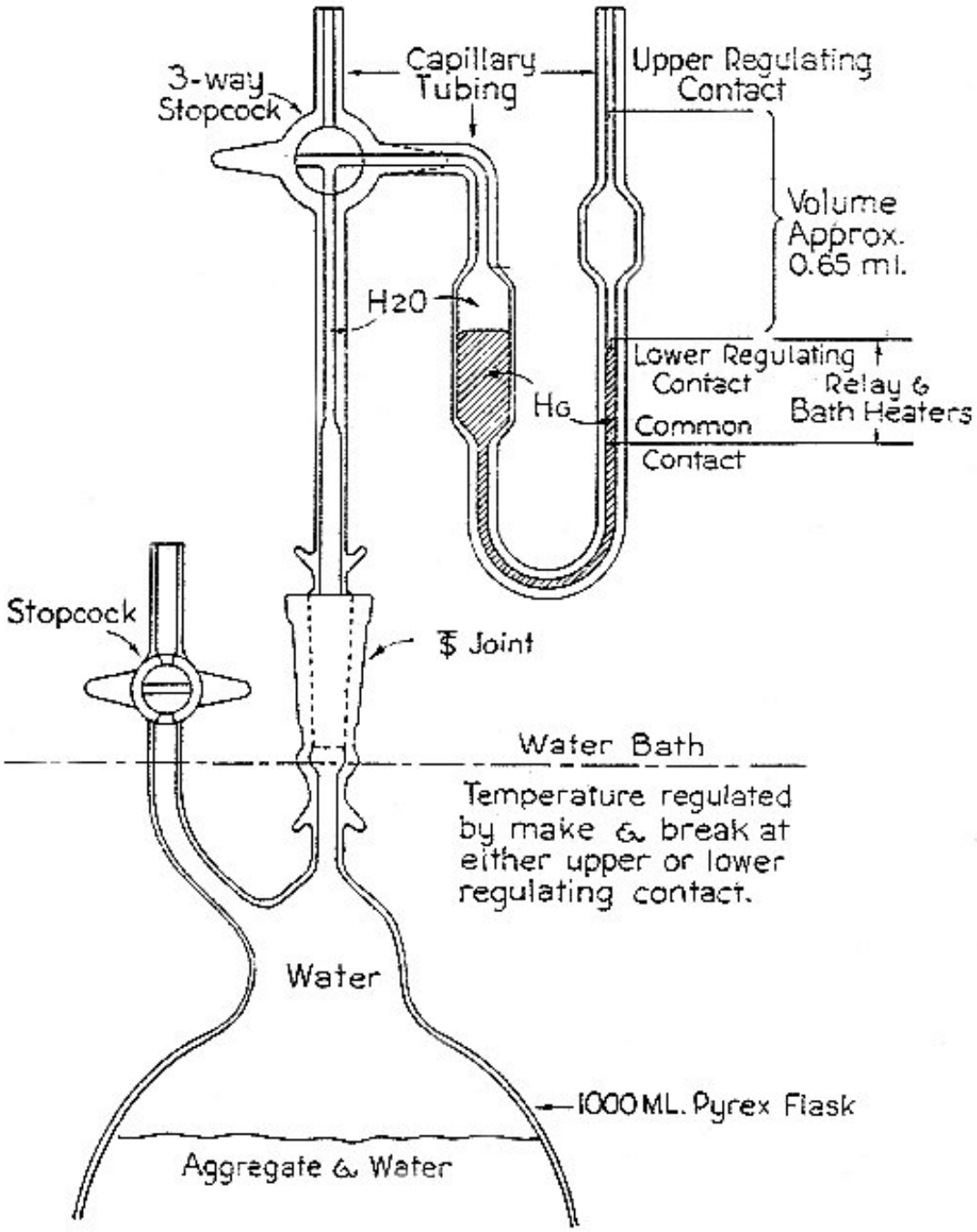

Figure 7. Dilatometer Developed by Verbeck and Haas (22).

characteristics of the aggregate. For measurements made below the freezing point of water, a non-reactive liquid, such as toluene, which does not freeze at the desired temperature, could be substituted. It was fairly easy to prepare the sample for testing using dilatometry. In comparison to other methods, such as a mounted strain gage on a specific rock sample, this method has the advantage of testing aggregates of different sizes.

The Gnomix pvT high-pressure dilatometer (*23*) measures the change in volume of a specimen subjected to different temperatures and pressures. The Gnomix pvT apparatus (Figure 8) generates pressure-specific volume-temperature measurements using high-pressure dilatometry. Approximately 1 gram (0.0022 lb) of dry sample is loaded into a sample cell and placed in the pvT apparatus. The machine is brought to just below the melting point temperature; isothermal data acquisition begins as soon as the instrument is brought to this temperature. Volume readings are taken by a linear variable differential transducer (LVDT) for the specified temperature at pressures ranging from 10 to 200 MPa (1450-29000 psi). The procedure is repeated for decreasing temperatures, down to ambient temperature. Data may also be gathered while heating the specimen. From the gathered data, the volumetric expansion coefficient in the solid state is extracted.

Figure 8. Gnomix pvT High-Pressure Dilatometer (*23*).

AASHTO TP 60-00 Test Method

A test method was recently developed by AASHTO as test number TP 60-00, "Standard Test Method for the Coefficient of Thermal Expansion of Hydraulic Cement Concrete" (*24*). The procedure requires a 4 inch (10.2 cm) diameter core, cut to a length of 7 inches (17.8 cm) (Figure 9). The sample is saturated for more than 48 hours and then subjected to a temperature change of 40°C (104°F) in a water bath. The length change of the specimen is measured and, with the known length change of the measuring apparatus under the same temperature change, the COTE of the concrete specimen can be determined.

Figure 9. AASHTO TP-60-00 COTE Test Frame with LVDT.

PRESENT METHOD

For the present study researchers chose the dilatometer method to measure the COTE of coarse and fine aggregate and pure minerals. Substantial modification in the design of the dilatometer was made in comparison with the earlier version that Verbeck

and Haas used, though the basic working principle remains the same. The present data acquisition system is also entirely different than Verbeck and Hass's model (*22*). The present dilatometer developed at the Texas Transportation Institute (TTI) can accommodate all kinds of materials (e.g., loose coarse aggregate, fine aggregate, material of single mass with any size, core samples, etc.). A detailed description of the dilatometer used in the research is presented in the next section.

CHAPTER 4. COTE LABORATORY TESTING AND MODEL DEVELOPMENT

TESTING APPARATUS AND CALIBRATION

During this study the researchers developed a test apparatus referred to as a volumetric dilatometer for determining the bulk COTE of both fine and coarse aggregates. The method is particularly adaptable to the study of field-saturated coarse aggregates and sand and provides a means of testing a representative sample of a heterogeneous coarse aggregate.

Testing Apparatus

The dilatometer test device (Figure 10) consists of a stainless steel container, a brass lid with hollow tower, a glass float attached with a LVDT , a thermocouple, and a data acquisition system. The inner surface of the lid is configured at a certain angle so that entrapped air bubbles can easily move along the surface. A transparent window with graduations at different heights is placed along the side of the tower to set the water level.

The dilatometer container is filled with aggregate sample and water. The water level is fixed to a certain graduation mark in the tower. The dilatometer with the sample and water inside is placed in a water bath and allowed to experience temperature change through controlling the temperature of the water bath. Displacement of water due to thermal expansion of both tested material and water is recorded by the LVDT through the movement of the float, which is placed on the water surface in the tower. Electrical signals are generated by the LVDT as the core moves. The signals are acquired and amplified by a signal conditioner and then recorded by a computer data acquisition system. The LVDT used is a UCAS/sCHAEVITZ model MHR .050, which emits 10.00 V for a displacement of 1.27 mm (0.050 inch), which provides sufficient accuracy in the measurement of volume changes of the water surface in the tower.

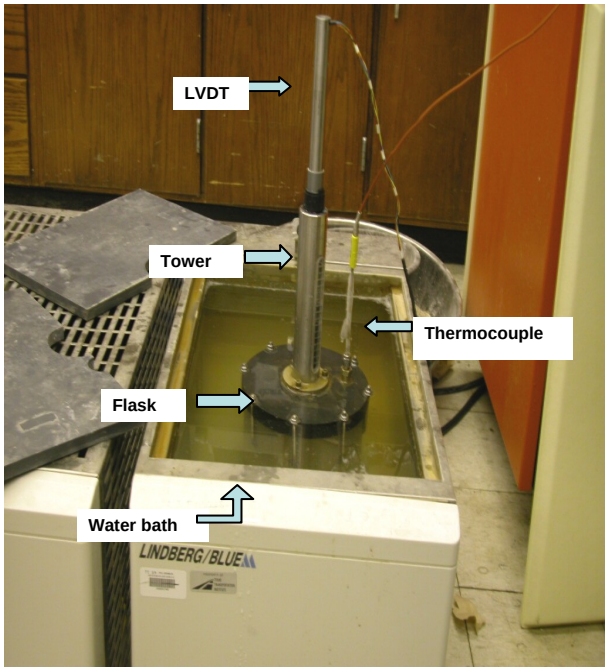

Figure 10. The Dilatometer Test Device.

The LVDT is calibrated to record 1/100 mm (0.0004 inch) of displacement. A thermocouple is inserted into the dilatometer through the tower to record the water temperature inside the container. The temperature and LVDT signals are continuously recorded by the same computer data acquisition system.

Dilatometer COTE measurement is basically an estimation of the COTE of the tested material based on the volumetric relationships between water, tested material, and container under a given temperature change. Research has shown that the linear COTE of an isotropic material is one-third the volumetric COTE (Appendix A) and for simplicity, the same is assumed for all tested materials.

Figure 11 represents the initial and final states of a dilatometer test. The container is filled with water and test sample so that the total initial and final volumes, V_1 and V_2, consist of the volume of water, V_w, and volume of aggregate sample, V_a, at each state. The instrumented system measures the displacement of water level, Δh, in the container tower with the change of temperature. These measurements produce an estimation of the COTE of aggregate sample based on the volumetric relationships between water, aggregate, and container at a given temperature change.

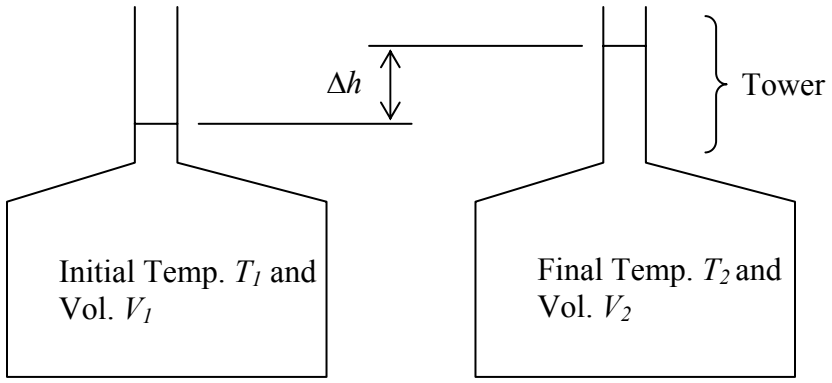

Figure 11. Initial and Final Stages of Dilatometer Testing.

In operation, the container is placed in the water bath and heated by the water surrounding it. When the temperature is raised from T_1 to T_2, the aggregate, the water, and the container all expand. Therefore, the apparent volume change that the LVDT detects consists of three parts:

$$\Delta V_1 = A\Delta h = \Delta V_a + \Delta V_w - \Delta V_f \qquad (4)$$

where ΔV_1 = observed total volumetric increase due to temperature change ΔT,
A = inner sectional area of tower,
Δh = rise of the water surface inside the tower,
ΔV_w = volumetric increase of water due to temperature ΔT,
ΔV_f = volumetric increase of inside volume of the dilatometer due to ΔT,
ΔV_a = volumetric increase of aggregate V_a due to ΔT, and
ΔT = temperature increase from T_1 to T_2.

Since

$$V_f = V_a + V_w = V \qquad (5)$$

$$\Delta V_a = V_a \gamma_a \Delta T$$

$$\Delta V_f = V \gamma_f \Delta T$$

$$\Delta V_w = V_w \gamma_w \Delta T = (V - V_a) \gamma_w \Delta T$$

where V = total inner volume of the flask,

V_w = volume of water in the flask,

V_f = volume of the flask,

V_a = volume of aggregate in the flask,

γ_a = coefficient of volumetric thermal expansion of aggregate,

γ_w = coefficient of volumetric thermal expansion of water, and

γ_f = coefficient of volumetric thermal expansion of flask.

The final equation to calculate the aggregate bulk COTE (γ_a) can be derived as

$$\gamma_a = \frac{1}{V_a}\left(\frac{A \cdot \Delta h}{\Delta T} - V_w \cdot \gamma_w + V_f \cdot \gamma_f\right) \quad (6)$$

where, $V_w = V - V_a = V_f - V_a$

The volumetric COTE of the tested aggregates is calculated by equation (6). Among the parameters on the right-hand side of the equation, the cross-sectional area of the tower, A, is a fixed known value for the dilatometer. The thermal coefficient of the container, γ_f, is estimated by calibration and is also a fixed parameter. Other parameters, Δh, T, V, V_a, and γ_w, are variable and they are measured/determined during the test matching with the test conditions. Close review of the determination of the above input values will help clarify the validity of equation (6).

Initial Total Volume

The initial total volume, V, consists of the volume of water and the volume of the aggregate. This initial total volume is equivalent to the initial volume of the dilatometer, V_f. The initial total volume, V or V_f, is determined by measuring the weight of the dilatometer filled with water at a fixed level. The initial total volume is now determined by multiplying the weight of water and the specific volume of water at the initial tested temperature (T_1). The weight of water is independent of temperature. Estimation of the specific volume of water at different temperatures is described later in the section in the discussion of the COTE of water.

Calibration of Apparatus

The dilatometer is calibrated to measure the thermal coefficient of the container (γ_f). This is necessary to separate the volumetric expansion of the water and the container from the volumetric expansion of the tested material.

The COTE of the Dilatometer

The purpose of calibration of the dilatometer is to determine the apparent coefficient of volumetric thermal expansion of the flask and to ensure that the variability from test to test is within acceptable limits. The calibration procedure is described in Appendix B in the form of a calibration protocol. The dilatometer is filled with distilled water and tested over a temperature range from 10°C (50°F) to 50°C (122°F) in order to estimate the COTE of the dilatometer container. In this case, the volumetric relation shown in equation (6) becomes

$$\gamma_f = \gamma_w - \frac{A \cdot \Delta h}{V} \cdot \frac{1}{\Delta T} \qquad (7)$$

where $V = V_f = V_w$ and

$V_a = 0$.

This calibration gives an apparent COTE of the dilatometer of 29.44×10^{-6}/°F ± 0.04101. Over the temperature range used for the calibration, the volumetric expansion of the dilatometer showed linear behavior; therefore, this value is regarded as a constant.

The COTE of Water

The volume change of water is known to be nonlinear with respect to temperature changes. Therefore, the thermal coefficient of water, γ_w, is variable with respect to the selected temperature for a test. This variable parameter γ_w can be determined from the density of water at different temperatures (from literature) and is presented in Table 7.

The reciprocal of the density gives the specific volume of water at different temperatures. The change in specific volume of water with temperature is shown in

Figure 12. As shown in the figure, the volumetric behavior of water under temperature change is perfectly fitted with a fourth-order polynomial equation. The specific volume

Table 7. Density of Water at Different Temperatures *(24)*.

Temp. (°C [°F])	Density (g/cm^3 [lb/ft^3])	Temp. (°C [°F])	Density (g/cm^3 [lb/ft^3])
0 (32)	0.99984 (62.420)	60 (140)	0.98320 (61.381)
10 (50)	0.99970 (62.411)	70 (158)	0.97778 (61.043)
20 (68)	0.99821 (62.318)	80 (176)	0.97182 (60.671)
30 (86)	0.99565 (62.158)	90 (194)	0.96535 (60.267)
40 (104)	0.99222 (61.944)	100 (212)	0.95840 (59.832)
50 (122)	0.98803 (61.683)		

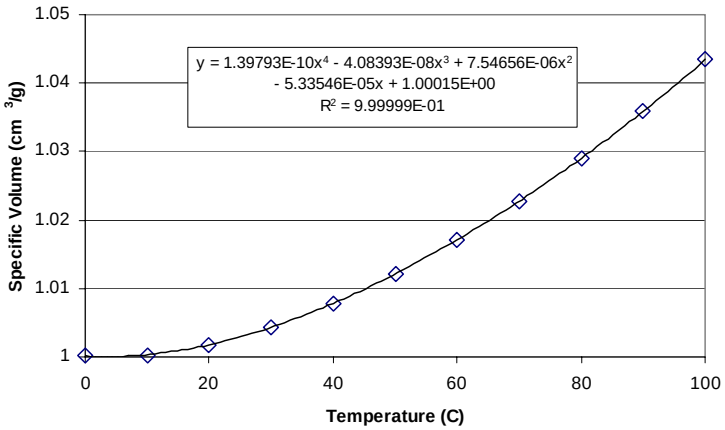

Figure 12. Thermal Expansion of Water.

of water at any given temperature from 0°C (32°F) to 100°C (212°F) can be estimated using the regression equation shown in Figure 12.

Now the volume change of water for any temperature change within the range of 0°C (32°F) to 100°C (212°F) can be obtained as:

$$\gamma_w = \frac{\Delta V}{V} \cdot \frac{1}{\Delta T} = \frac{W \cdot (v_2 - v_1)}{W \cdot v_1} \cdot \frac{1}{\Delta T} = \frac{v_2 - v_1}{v_1 \cdot (T_2 - T_1)} \quad (8)$$

where V = initial volume of water,

ΔT = change of temperature from T_1 to T_2,

ΔV = change of volume of water due to the temperature change, and

W = weight of water, and

v_1 and v_2 = specific volumes of water at temperatures T_1 and T_2, respectively.

Estimation of Error

Calibration with respect to separation of the volumetric expansion of the water and the container from the volumetric expansion of the tested material removes the possible systematic error. The thermal coefficient of the dilatometer is a constant parameter as long as the shape, size, and material of dilatometer remain the same. However, random error may exist in the test protocol. Error and sensitivity are evaluated with respect to the determination of input parameters and subsequent calculation of the COTE of aggregate. Random error may exist in determining the initial volume of aggregate associated with the measurements of the weight of aggregate. The effect of error in weight on the determination of volume is not significant. However, it should be recognized that the initial volume of aggregate could influence the determination of the aggregate COTE, as previously noted. Considering that, in general, 3300-3700 g (7.3-8.2 lb) of saturated surface dry aggregate is used for a normal COTE test, it is expected that the maximum random error in measuring the weight of aggregate would not be more than 5 g (0.125 percent).

The sensitivity of the measurements on Δh is greater than other parameters. Considering that the general range of Δh is determined to be 15 mm (0.591 inch) to 20 mm (0.787 inch), an error of only a few tenths of a millimeter produces significant error. The LVDT was calibrated to record 1/100 mm (0.0004 inch) of displacement, which is in the range of its precision. It should be recognized that the thermal coefficient of water is much higher than the coefficient of the aggregate sample, so the majority of the volumetric expansion is governed by water. Table 8 presents a summary of possible sources of random errors and their significance. Appendix C provides the details of variance analysis done on these factors.

Table 8. Possible Random Errors and Their Significance.

Sources of Random Errors	Coefficient of Variation of γ_a
Weight of aggregate	2.4%
Displacement reading (Δh)	4.0%-7.0%

Verification of the Test Method

As previously noted, measurement errors associated with float displacement and initial aggregate weight cause errors in determining the COTE of aggregate. In order to develop a procedure to reduce the calculated error, the research team conducted a series of verification tests such as:

1. Comparing the test result from the dilatometer with the result from strain gage setups for samples with known COTE values.
2. Checking the repeatability of the dilatometer tests with the same aggregate sample.
3. Tracking the data at a constant temperature condition to see if any systematic problems exist in the dilatometer test setup.

Tests for Steel and Glass Samples

The COTE of steel rod and glass rod samples (as standard reference materials) were determined by both dilatometer and strain gage methods. A favorable comparison between the dilatometer COTE and strain gage COTE of the tested reference materials

(e.g., steel or glass) has been considered as a validation for the dilatometer test method. The steel and glass rods were specially prepared at 1 to 2 cm (0.394 to 0.787 inch) diameter and 15 cm (5.906 inch) length.

Table 9 shows the results of dilatometer tests for the steel rods. T_1, T_2, and Δh represent the measured initial and final temperatures and displacement of water, respectively. The actual temperature readings from the inside of the dilatometer are noted in the table. Figure 13 shows actual data readings from test number 1 as a typical example of data measurements from the dilatometer.

Table 9. Dilatometer Test Results for the Steel Rod Samples.

Test No.	T_1 (°C[°F])	T_2 (°C[°F])	Δh (mm [inch])	COTE ($\times 10^{-6}$/°F)	Remarks
1	10.38 (50.68)	50.33 (122.60)	14.573 (0.574)	6.41	Average: 6.19 St Dev. (SD): 0.278
2	10.47 (50.85)	50.40 (122.72)	14.993 (0.590)	6.29	
3	10.50 (50.90)	50.41 (122.74)	14.809 (0.583)	5.88	

Figure 14 shows the results of two sets of tests using a strain gage method. Linear expansion of the steel bar was measured by the attached strain gage and relevant data logging device while temperature varies between -13°C and 22°C (8.6°F and 71.6°F). A separate thermocouple was attached to the surface of the steel rod to measure the actual steel temperature. As shown in Figure 14, thermal expansion of the steel rod was linear. Therefore, the COTE of the steel rod can be estimated as the slope of the best-fit line. The COTE of steel rods was determined to be 6.24×10^{-6}/°F with 5.76 percent covariance. As seen in Table 9, the average COTE of steel rods obtained from the dilatometer tests was 6.19×10^{-6}/°F with 4.49 percent covariance. These two results support each other; the difference of the two results is less than 1 percent.

For verification, the same comparative tests were conducted with glass rod samples. Table 10 shows the comparison of the results from the two different tests. The average COTE of glass rods obtained by the two dilatometer tests is 4.59×10^{-6}/°F, and the difference between this and the strain gage test result is 1.8 percent. As presented,

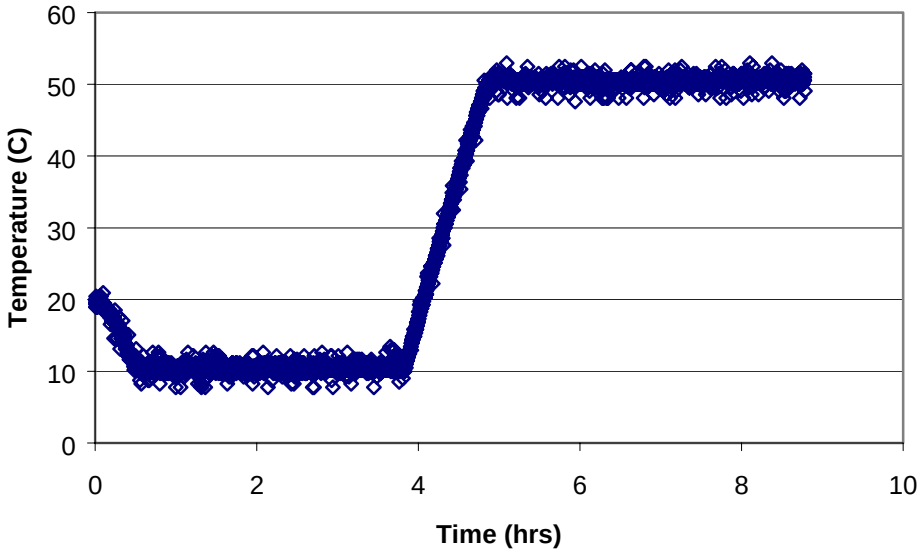

(a) Temperature measurements

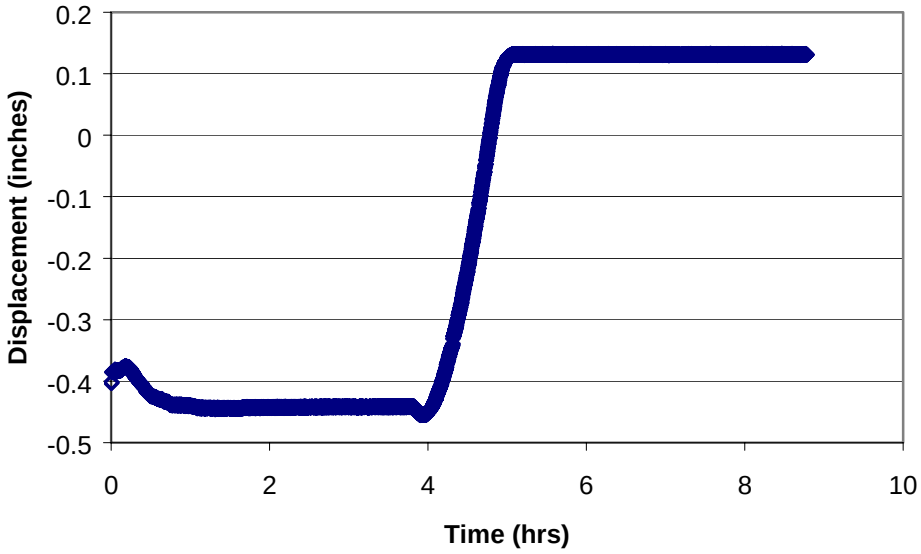

(b) Corresponding displacement of the water level at the tower of dilatometer

Figure 13. Typical Data Measurements of Dilatometer Tests.

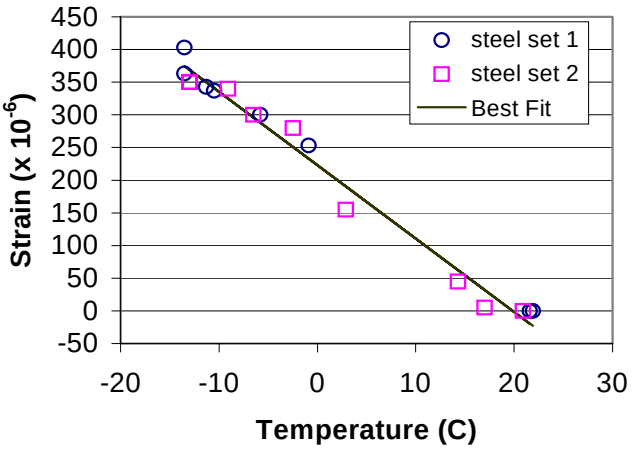

Figure 14. Thermal Expansions of Steel Rod Samples Measured by Strain Gage (COTE = 6.24 × 10^{-6}/°F, SD = 0.36, R^2 = 0.983).

Table 10. Comparison of COTE of Glass Rods Obtained by Dilatometer and Strain Gage.

Test	T_1 (°C [°F])	T_2 (°C [°F])	COTE (× 10^{-6}/°F)
Dilatometer 1st	10.35 (50.63)	50.45 (122.81)	4.70
Dilatometer 2nd	10.28 (50.50)	50.31 (122.56)	4.49
Strain Gage	-13.6 (-56.48)	21.3 (70.34)	4.68

both steel and glass rod test results strongly support the reliability of the dilatometer test protocol.

Repeatability of Dilatometer Tests in Measuring Aggregate COTE

It is to be mentioned that the above verification tests using steel and glass rods indicated good repeatability for the reference materials. In this section, repeatability of the dilatometer test protocol was investigated by repeating the test three times for a single aggregate (Abilene limestone) sample. The results are compared and presented in Table 11. The initial sample weight was in saturated surface dry (SSD) condition, and the volume ratio represents the ratio of initial volume of aggregate sample (V_a) to the initial

total volume (V). The dilatometer was not opened between tests 2 and 3 and was left in the water bath until it cooled to room temperature so that the same sample was used for the last two tests. Note that the initial volumetric relations are different even for those two tests because the measured initial temperatures were slightly different. Comparison of repeated test results indicated that the dilatometer produces acceptable repeatability. The average COTE of the three tests is 3.36×10^{-6}/°F with 4.34 percent coefficient of variance (COV).

Table 11. Comparison of Repeated COTE Tests for Abilene Limestone.

Test	Initial sample weight (g)	Volume ratio (V_a/V)	T_1 (°C [°F])	T_2 (°C [°F]	Δh (mm [inch])	COTE ($\times 10^{-6}$/°F)
1	3967.2	0.4937	10.45 (50.81)	50.42 (122.76)	16.701 (0.658)	3.21
2	4054.4	0.5044	10.55 (50.99)	50.71 (123.28)	16.601 (0.654)	3.56
3	4054.4	0.5055	10.41 (50.74)	50.58 (123.04)	16.381 (0.645)	3.32

Tests at Constant Temperature Conditions

Possible systematic errors that may involve in the test method were investigated by testing under two different constant temperature conditions. In the first test, the dilatometer filled with water and aggregate sample was placed in the water bath, which was maintained at a temperature of 35°C (95°F). The data were collected as a normal COTE test but over a longer period of time. The test result indicated that at least 2 hours of resting time was required after the final temperature was reached to get stable LVDT data. However, the maximum rebound of LVDT data is about 0.05 mm (0.002 inch), from which the resultant error in COTE is less than 2 percent. For a normal COTE test, the displacement is averaged for at least 30 minutes between 1.5 and 2 hours after the final temperature is reached. According to the trend of the LVDT data, the current data reduction method seems to be reasonable.

In the second test, the dilatometer was placed in the water bath at room temperature without operating the water bath and data were collected for 11 hours. The

slight decrease in measured temperature is believed to be caused by the decrease of the room temperature during the night. The trend of the data shows (Figure 15) the conformity between test volume and temperature.

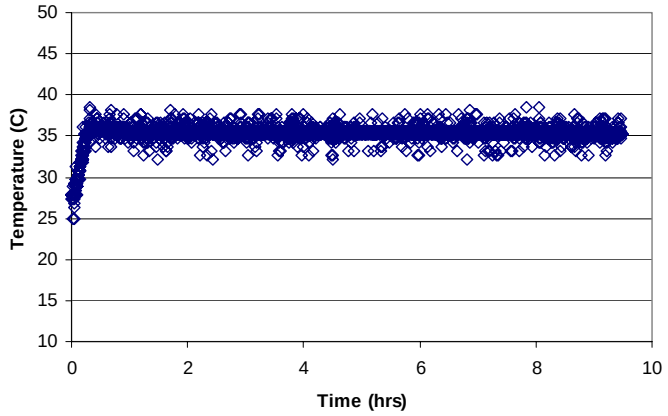

(a) Temperature data

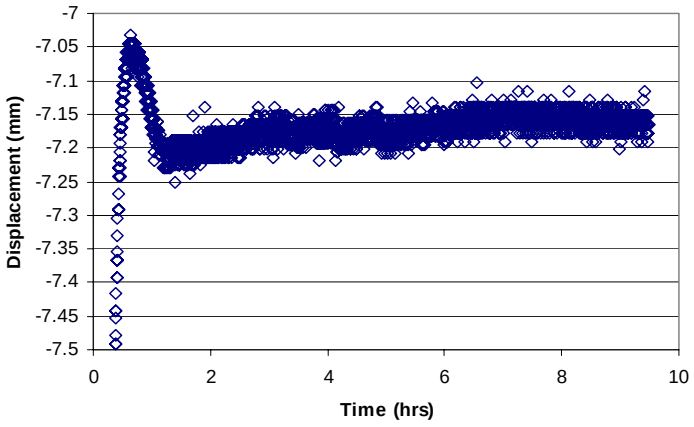

(b) LVDT data

Figure 15. Data Collection at a Constant Temperature (35°C/95°F, 1 mm = 0.039 inch)

LABORATORY TEST PROGRAM

There are four steps in the volumetric dilatometer test:

1. preparing the sample,
2. vacuuming/de-airing,
3. testing, and
4. analyzing the results.

Preparing the Sample

A representative aggregate sample, one and one-half times the required volume, is selected. The sample is properly washed to remove dust and unwanted particles and is then submerged in water for at least 24 hours before starting the test. After the sample is taken out of water it is washed once again before placing it inside the dilatometer. The SSD and the submerged weight of aggregate are determined following ASTM specifications C-127 and C-128. The volume of aggregate (V_a) at the initial testing temperature (i.e., 10°C) is calculated using the equation below:

$$V_a = v \cdot (W_{SSD} - W_{SUB}) \tag{9}$$

where

v = specific volume of water at the initial testing temperature,
W_{SSD} = weight of the aggregate sample in saturated surface dry condition, and
W_{SUB} = weight of aggregate sample submerged under water.

In equation (9), the temperature dependence of the aggregate volume is accounted by the specific volume of water at the specific temperature. The weights are independent of temperature.

The whole dilatometer is then filled with the aggregate sample. The lid of the dilatometer is screwed tightly, and it is then filled with water to a certain level marked on the lid window.

De-airing

De-airing is performed based on the guidelines provided in Appendix D.

Testing

The water level is set to the fixed position after vacuuming. The dilatometer is then placed into the 24°C (75.2°F) water bath. The LVDT housing is placed on the LVDT rod, which is connected to the float through a threaded rod. The smooth float placement on the water surface is ensured by rotating the LVDT housing hollow pipe and observing the change in LVDT reading on the computer monitor. A steady LVDT reading while slowly rotating the LVDT housing is an indication for better placement of LVDT housing on top of the float. The LVDT readings are monitored for an additional 15 minutes to make sure that there is no leak from the dilatometer. Then the water bath temperature is adjusted to the initial temperature (T_1), i.e., 10°C (50°F). It takes around 0.5 hour to reach 10°C (50°F). An additional 1.5 hours is necessary for the whole system (especially aggregate and water inside dilatometer) to stabilize at 10°C (50°F). The data acquisition system automatically records the initial water temperature inside the dilatometer container and the position of the water surface (h_1). The initial displacement (h_1) and temperature (T_1) are the average of at least 30 minutes displacement and temperature data between 1.25 and 1.75 hours after starting the test. Then the temperature is changed to the final temperature (T_2), i.e., 50°C (122°F). The position of the water surface at temperature T_2, denoted by h_2, is recorded by the LVDT and the data acquisition system. The final displacement (h_2) and temperature are the average of at least 30 minutes data between 1 and 2 hours after the final temperature is reached. Consequently, the rise of the water surface when temperature is increased by ΔT from T_1 to T_2 is $\Delta h = h_2 - h_1$.

Analysis

The coefficient of thermal expansion of the tested aggregate can be calculated using equation (6) with measured values of aggregate volume at initial testing temperature (V_a), volume of the flask (V), displacement ($\Delta h = h_2 - h_1$), temperature difference ($\Delta T = T_2 - T_1$), coefficient of volume expansion of water (γ_w), and coefficient

of volume expansion of container (γ_f, 29.44 × 10^{-6}/°F, *assigned by doing calibration).* The whole calculation procedure is programmed in an Excel spread sheet and submitted to TxDOT. The dilatometer-measured COTE values of the different types of aggregates are presented in a later section.

MODELING APPROACH

Basically, two models predict the properties of a composite from those of its components: the parallel model and the series model. In the parallel model, the components of a composite are assumed to be combined in parallel. In the case of concrete, cement mortar and aggregate are the parallel components, as shown in Figure 16(a). When the concrete is loaded, mortar and aggregate are both displaced, so that the strain in both the components is the same. The series model is illustrated in Figure 16(b), where the total displacement of the concrete under a tension force is the sum of the displacement of the constituent mortar and aggregate. The stress in the constituent mortar and aggregate is uniformly distributed. Hirsch's model (*8*) is a combination of the above two models, which has been used to predict the elastic modulus of concrete (Figure 16[c]). The present aggregate and concrete COTE model is based on the concept of Hirsch's composite model.

Constituent minerals in the aggregate are the components in the aggregate COTE model, whereas mortar and coarse aggregate are the components in the concrete COTE model. The derived formulae for the aggregate and concrete COTE models based on Hirsch's composite model are presented later.

MODELING OF AGGREGATE COTE

A model is proposed to predict aggregate COTE based on the calculated mineral weight percentages, measured pure mineral COTE, and their modulus of elasticity (MOE) (*25, 26*). Minerals present and their respective weight percentages in the aggregates are calculated from the bulk chemistry (i.e., elemental oxide weight percentages of the aggregates). COTE of common pure minerals was measured by dilatometry, and MOE of minerals was collected from literature (*27*, *28*). The prediction

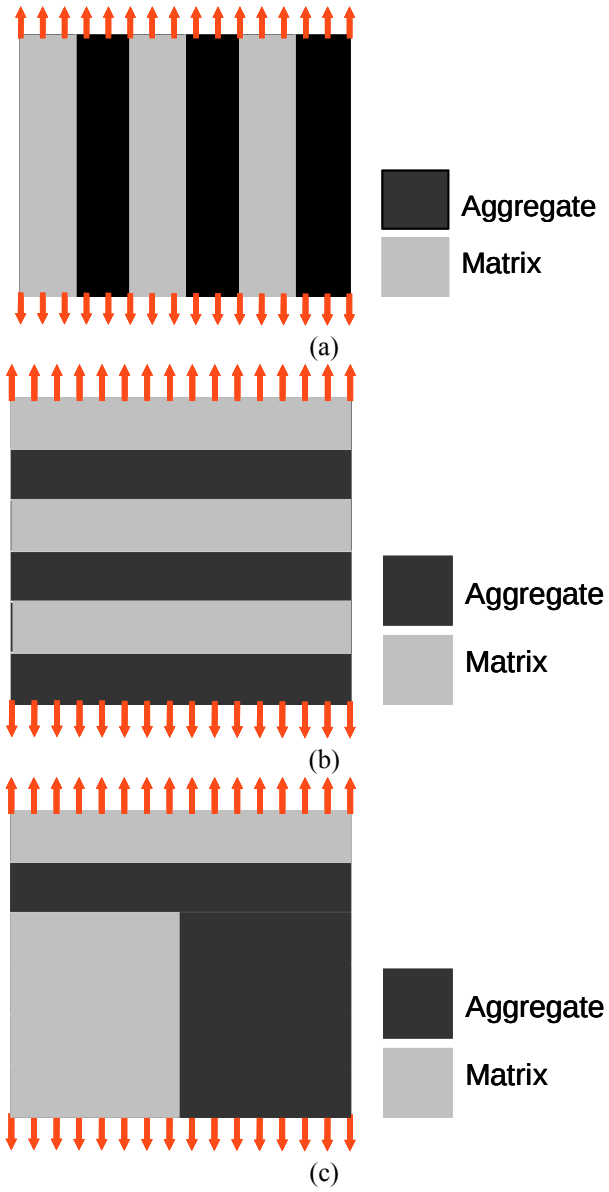

Figure 16. Composite Models for Concrete COTE Calculation: (a) Parallel Model, (b) Series Model, and (c) Hirsch's Model.

model for the aggregate COTE is then formulated based on Hirsch's composite model *(8)*.

Materials and Test Methods

Five different types of commonly used aggregates, namely, siliceous river gravel (SRG, Fordyce), calcareous river gravel (CRG, mainly calcareous with siliceous impurities, Trinity), pure limestone (Vulcan), sandstone (Martin Marietta), and granite (Martin Marietta) were collected from different areas across the state of Texas. COTE was determined by dilatometry on samples of five pure minerals, namely, calcite, quartz, dolomite, albite (Na-feldspar), and microcline (K-feldspar) obtained from Ward's Natural Science Est. Inc. These five minerals represent, to a large extent, the expected mineralogy of the above aggregates. The effect of other commonly occurring minor minerals (e.g., pyroxenes, magnetite/hematite, micas) on aggregate (e.g., granite) COTE was assumed to be insignificant. Bulk chemical analyses of representative powder samples of the above aggregates were carried out by X-ray fluorescence (XRF) at Wyoming Analytical Laboratories, Inc., located in Golden, Texas. Calculated mineralogy obtained by the proposed model (discussed later) for each aggregate was verified by X-ray diffraction (XRD, Rigaku Miniflex) at TTI. Concrete cylinders of 8 × 4 inches (20.3 × 10.2 cm) were cast using the above-mentioned coarse aggregates, fine aggregate (single source), Type I cement, and fly ash with 0.42 water/(cement + fly ash) ratio. A standard mortar using the same sand and maintaining the same ratio of sand : cementitious materials in concrete was cast. Dilatometry was used to measure the COTEs of the individual pure minerals, above-mentioned aggregates, mortar, and concrete. Cylindrical mortar and concrete specimens (5.6 × 4 inch [14.2 × 10.2 cm]) were obtained from the original 8 × 4 inch (20.3 × 10.2 cm) specimens, and measurement of COTE by dilatometer was performed after 28 days of moist curing. Representative samples from as-received loose aggregate were prepared and used to measure aggregate COTE.

Sample Preparation

Obtaining a representative powder sample from a bulk aggregate sample is an important step for effective mineralogical COTE characterization. A sampling protocol

was introduced to obtain a representative aggregate powder sample (Appendix E). Representative powder samples for all collected aggregate samples were prepared following the above guidelines. Elemental oxide weight percentages for all prepared aggregate powder samples were determined by XRF and are presented in Table 12.

Table 12. Bulk Chemical Analyses of the Tested Aggregates.

Aggregate	Sample No.	Bulk chemical analyses (wt%)							
		SiO_2	Al_2O_3	Fe_2O_3	CaO	MgO	Na_2O	K_2O	LOI
Gravel (siliceous), **SRG**	1	94.17	0.93	0.94	1.78	0.00	0.22	0.28	1.68
	2	96.86	0.79	1.01	0.54	0.11	0.00	0.14	0.55
Gravel* (calcareous), **CRG**	3	35.57	1.20	2.30	32.20	1.50	0.00	0.30	26.46
	4	22.13	0.29	2.72	40.31	1.39	0.00	0.24	32.67
Limestone (**LST**)	5	2.28	0.47	0.24	53.76	0.52	0.00	0.05	42.53
	6	0.26	0.11	0.04	55.33	0.39	0.01	0.01	43.73
	7	2.57	0.24	0.65	53.07	0.61	0.00	0.07	42.39
	8	5.97	0.23	0.86	51.07	0.86	0.00	0.07	40.92
	9	6.21	0.11	0.06	51.53	0.86	0.05	0.01	41.17
	10	0.34	0.00	0.08	54.16	1.67	0.08	0.02	43.65
	11	0.24	0.00	0.03	56.16	0.15	0.00	0.00	43.42
Sandstone (**SST**)	12	79.84	8.43	4.51	1.09	0.85	1.43	1.95	1.67
	13	90.16	2.70	3.28	0.62	0.22	0.30	0.58	2.13
Granite (GRN)	14	72.14	13.62	3.28	1.24	0.28	3.86	4.92	0.02
	15	68.97	13.45	5.21	2.18	0.80	3.72	4.23	0.21

* mainly calcareous with siliceous impurity. LOI = loss on ignition.

Determination of Mineral Weight Percentages from Bulk Chemical Analysis

As previously noted, minerals present in an aggregate source and their respective weight percentages can be estimated from the elemental oxides as determined by chemical analyses. Two different schemes of calculation (method I and method II) were proposed to determine mineral weight percentages from bulk chemical analysis of aggregate. These calculations apply to a wide range of rocks (i.e., sedimentary, igneous, and their metamorphic equivalents) commonly used as aggregates and provides a realistic representation of the mineral phases present in different types of aggregate.

Method I

This method was used to calculate weight percentages of seven minerals (dolomite, albite, orthoclase, anorthite, quartz, calcite, and magnetite) and is applicable to aggregates belonging to the sedimentary group of rocks and their metamorphic

equivalents (e.g., limestone, gravel, sandstone, marble, etc.). These seven minerals cover the major constituents in most sedimentary rocks and their metamorphic equivalents, which are commonly used as aggregates. This calculation method is based on an allotment of elemental oxide weight percentages to mineral weight percentages according to stoichiometric chemical equations for minerals (Table 13). This method is not used for shale, siltstone, or schist rocks because of limitations in calculating the micaceous and clay minerals. However, the practice of using these types of rocks as concrete aggregate is somewhat limited. The following assumptions were considered for simplification of the calculation (Table 13):

- All SiO_2 is allocated to quartz and feldspar. The three most commonly occurring types of feldspar (i.e., potassium feldspar [orthoclase/microcline], sodic feldspar [albite] and calcium feldspar [anorthite]) are considered for the calculation.
- All CaO is allocated to calcite, dolomite (to combine all MgO), and anorthite (to combine, if any, leftover Al_2O_3 after orthoclase and albite).
- All Fe_2O_3 is allocated to magnetite or hematite because chemical analysis generally includes all Fe in Fe_2O_3 or FeO.

Table 13. Derived Formulas to Calculate Weight Percentages of Minerals from Aggregate Bulk Chemical Analysis by Method I.

Minerals	Chemical formula of minerals	Formulas to calculate mineral weight % based on equations in column 4	Stoichiometric equations
Dolomite (g), Do	$(Ca,Mg)(CO_3)_2$	$= MgO \times 4.5752$	$CaMg(CO_3)_2 \rightarrow CaO + MgO + 2CO_2$
Albite (g), Ab	$NaAlSi_3O_8$	$= Na_2O \times 8.46$	$Na_2Al_2Si_6O_{16} \rightarrow Na_2O + Al_2O_3 + 6SiO_2$
Orthoclase (g), Or	$KAlSi_3O_8$	$= K_2O \times 5.80$	$K_2Al_2Si_6O_{16} \rightarrow K_2O + Al_2O_3 + 6SiO_2$
Anorthite (g), An	$CaAl_2Si_2O_8$	$= 2.7287(Al_2O_3 - Ab \times 0.1944 - Or \times 0.1832)$	$CaAl_2Si_2O_8 \rightarrow CaO + Al_2O_3 + 2SiO_2$
Quartz (g), Qtz	SiO_2	$= SiO_2 - Ab \times 0.6874 - Or \times 0.6595 - An \times 0.4363$	
Calcite (g), Cc	$CaCO_3$	$= 1.785(CaO - Do \times 0.3041 - An \times 0.2016)$	$CaCO_3 \rightarrow CaO + CO_2$
Magnetite (g), Mt	Fe_3O_4	$= Fe_2O_3 \times 1.4499$	$Fe_3O_4 \rightarrow FeO + Fe_2O_3$

Method II

This method is used to calculate weight percentages of nine minerals (apatite, ilmenite, orthoclase, albite, anorthite, pyroxenes, olivine, quartz, and magnetite/hematite) and is applicable to aggregates belonging to the igneous suite of rocks and their metamorphic equivalents (e.g., granite, basalt, granulites, and ultrabasic rocks, etc.). Method I cannot be used to calculate the mineralogy of these rocks because:

- The allotment of SiO_2 only to feldspars and quartz (method I) is not valid for these rock types. Ferromagnesian silicates (e.g., pyroxene, olivine) are essential mineral phases in these suites of rocks, and they also contain SiO_2. Ultrabasic rocks do not contain quartz, which can only be reflected by method II.
- Calcite and dolomite are not present in the igneous suite of rocks as a primary crystallizing phase. Therefore, allotment of CaO to calcite and dolomite is not valid for these groups of rocks where the primary source of CaO is Ca-feldspar (anorthite) with minor contributions from pyroxenes (e.g., diopside) and amphiboles.

The calculation of method II is based on proper sequential allotment of the molecular proportion of elements to mineral weight percentages based on the crystallization sequence in magma. Detailed steps for the calculation of method II are presented in Table 14.

The following selection criteria are provided to determine the suitable method for the sampled aggregate based on bulk chemical analysis:

- $SiO_2 \geq 80$ percent (e.g., sandstone, fine sand aggregates, siliceous gravel, metaquartzite, etc.) - method I.
- $CaO \geq 30$ percent and $LOI \geq 25$ percent (e.g., limestone, marble, etc.) - method I.
- $SiO_2 = 38\text{-}75$ percent, $Al_2O_3 = 10\text{-}18$ percent, and $CaO < 20$ percent (igneous rocks, e.g., granite, rhyolite, andesite, diorite, basalt, gabbro, etc.) - method II.

The proposed methods were applied to calculate mineral weight percentages from bulk chemical analysis of the respective aggregate powder samples and are presented in Table 15. Table 15 also shows the presence of actual minerals identified by XRD. A perusal of Table 15 shows that calculated mineralogy based on the proposed method closely

resembles the actual mineralogy identified by XRD. This supports the feasibility of the proposed method to calculate the mineralogy in a realistic manner.

Table 14. Sequential Allotment of Elemental Oxide Weight Percent to Mineral Weight Percentages for Method II.

Calculation of molecular proportion (MP): divide the weight percentage (wt%) of each oxide by its molecular weight to find the molecular proportion of that oxide			
Minerals	**Chemical Formula**	**Equations to Calculate MP for Minerals**	**Residual elemental Oxide Weight Percent after Formation of a Particular Mineral**
Apatite	$Ca_5(PO_4)(OH,F,Cl)$	= MP of P_2O_5	$CaO_I = CaO_t - 3.33 \times$ MP for apatite
Ilmenite	$FeTiO_3$	= MP of TiO_2 if $FeO > TiO_2$	FeO_I = MP of FeO_t – MP of TiO_2
Orthoclase (K-feldspar)	$KAlSi_3O_8$	= MP of K_2O	$Al_2O_3(I)$ = MP of $Al_2O_{3(t)}$ – MP of K_2O $SiO_2(I)$ = MP of $SiO_{2(t)}$ – 6 × MP of K_2O
Albite (Na-feldspar)	$NaAlSi_3O_8$	= MP of Na_2O	$Al_2O_3(II) = Al_2O_3(I)$ – MP of Na_2O $SiO_2(II) = SiO_2(I) - 6 \times$ MP of Na_2O
Anorthite (Ca-feldspar)	$CaAl_2Si_2O_8$	= $Al_2O_3(II)$ if $CaO_I > Al_2O_3(II)$	$CaO_{II} = CaO_I - Al_2O_3(II)$ $SiO_2(III) = SiO_2(II) - 2 \times Al_2O_3(II)$
Anorthite	$CaAl_2Si_2O_8$	= CaO_I if $CaO_I < Al_2O_3(II)$	$Al_2O_3(III) = Al_2O_3(II) - CaO_I$ $SiO_2(III) = SiO_2(II) - 2 \times CaO_I$
Corundum	Al_2O_3	= $Al_2O_3(III)$	
Magnetite	Fe_3O_4	= FeO_I if $Fe_2O_{3(t)} > FeO_I$	$Fe_2O_3(I) = Fe_2O_{3(t)} - FeO_I$
Magnetite	Fe_3O_4	= MP of $Fe_3O_{4(t)}$ if $Fe_2O_{3(t)} < FeO_I$	$FeO(II) = FeO_I - Fe_3O_{4(t)}$
Hematite	Fe_2O_3	= $Fe_2O_3(I)$	
Diopside (Pyroxene)	$(Ca,Mg)Si_2O_6$	= CaO_{II}	$(MgO + FeO)_R$ after diopside = $(MgO_t + FeO_{II}) - CaO_{II}$ $SiO_2(IV) = SiO_2(III) - 2 \times CaO_{II}$
Hypersthene (Pyroxene)	$(Fe,Mg)SiO_3$	= $(MgO + FeO)_R$ if diopside is "YES"	$SiO_2(V) = SiO_2(IV)$ – MP for hypersthene
Hypersthene	$(Fe,Mg)SiO_3$	= $(MgO_t + FeO_{II})$ if diopside is "NO"	$SiO_2(V) = SiO_2(IV)$ – MP for hypersthene
Quartz	SiO_2	= $SiO_2(V)$	
Multiplication of the above molecular proportions assigned to the respective phases by their molecular weight will give the weight % of respective minerals.			

MP – Molecular proportion, t / (t) – total

Table 15. Calculated Mineral Volume (Percent) by the Proposed Methods for the Tested Aggregates along with Actual Minerals Identified by XRD for Some Selected Aggregates.

Aggregate	Samp No.	Mineral Volume (%)								Minerals identified from XRD
		Do	Cc	Ab	An	Pf	Qtz	Mt	Pyx	
SRG **METHOD I**	1	0.00	02.73	01.91	00.69	01.71	92.25	0.69	0.00	Qtz
	2	0.47	00.06	00.00	01.69	00.85	96.18	0.75	0.00	
CRG **METHOD I**	3	6.71	51.92	00.00	02.44	01.90	35.23	1.79	0.00	
	4	6.27	67.50	00.00	00.01	01.37	20.87	3.88	0.00	Cc, Qtz, Ab (t), Do (t)
Limestone **METHOD I**	5	2.37	94.23	00.00	01.17	00.32	01.71	0.19	0.00	
	6	1.77	97.73	00.09	00.24	00.06	00.07	0.03	0.00	Cc, Ab (t), Do (t)
	7	2.80	93.29	00.00	00.45	00.41	02.11	0.94	0.00	
	8	3.92	88.58	00.00	00.44	00.45	05.92	0.68	0.00	
	9	3.90	89.22	00.46	00.05	00.06	06.26	0.05	0.00	
	10	7.57	91.96	00.73	00.00	00.13	00.00	0.06	0.00	Cc, Ab (t), Do (t)
	11	0.68	99.04	00.00	00.00	00.00	00.26	0.02	0.00	
Sandstone **METHOD I**	12	3.56	00.00	12.13	10.46	11.60	58.95	3.31	0.00	
	13	0.96	00.00	02.66	04.29	03.61	86.93	2.51	0.00	
Granite, **METHOD II**	14	0.00	00.00	32.66	05.31	29.08	24.85	0.00	6.29	Qtz, Ab, Pf, Pyx, Biotite, Muscovite
	15	0.00	0.00	31.48	7.50	25.00	22.33	0.00	11.31	

D – Dolomite, Cc – Calcite, Ab – Albite (Na-feldspar), Pf – K-feldspar, Qtz – Quartz, Mt – Magnetite, Pyx – Pyroxene, t – trace amount

COTE of Pure Minerals

The COTE of five natural pure minerals (calcite, dolomite, albite, orthoclase, and quartz) were measured by dilatometry and are presented in Table 16. These five pure minerals constitute the majority of expected mineralogy of the tested aggregates. The cylindrical 5.6 × 4 inch (14.2 × 10.2 cm) specimens were obtained from larger mineral samples by coring and were placed in the dilatometer for testing. Calcite, dolomite, and quartz were polycrystalline type, whereas albite and orthoclase were selected from cleaved blocks. Powder samples of all the collected minerals were prepared and analyzed by XRD to check their purity. The minor phases identified as impurities are also listed in Table 16. Note that the minerals in natural aggregates also contain similar types of impurities. The feldspar group of minerals always occurs as a solid solution of two or three end-members

and never occurs as a single pure end-member. Therefore, the measured COTE of these naturally occurring minerals with traces of impurities provides a more realistic mineral COTE input for the aggregate COTE modeling. The COTE of some of these minerals were obtained from literature (*28*, *29*) and are included in Table 17 for comparison. An overall resemblance between measured dilatometer COTE and COTE obtained from literature is evident.

Table 16. COTE of Pure Minerals Measured by Dilatometer, Their Respective Elastic Modulus, and Phases Identified as Impurities by XRD.

Minerals	COTE Measured (10^{-6}/°F)	COTE from Literature *(28)* (10^{-6}/°F)	Elastic Modulus (× 10^6 psi) *(28)*	Traces of Minerals Identified as Impurity by XRD
Calcite	3.10		20.42	No impurity
Dolomite	5.34		29.07	1. Ankerite [Ca(Fe,Mg)(CO_3)] 2. Minrecordite [CaZn(CO_3)]
Quartz	7.22		12.30	No impurity
Microcline	3.67		9.50	Disordered albite ($NaAlSi_3O_8$)
Albite	3.78		10.50	Anorthite ($CaAl_2Si_2O_8$)
Anorthite		2.61	17.60	Albite ($NaAlSi_3O_8$)
Magnetite	—	3.81	38.30	
Pyroxene	—	6.73	32.50	

Composite Modeling to Predict Aggregate COTE

The model to predict aggregate COTE is based on the concept of Hirsch's composite model (*8*), where determined COTE of pure minerals and their respective volume percent are the two main inputs. The following formula is adopted based on Hirsch's composite modeling to predict aggregate COTE (*30*):

$$\alpha_a = x\sum \alpha_i V_i + (1-x)\left\{\frac{\sum \alpha_i V_i E_i}{\sum V_i E_i}\right\} \qquad (10)$$

where

α_a = COTE of aggregate,

α_i = COTE of individual mineral,

V_i = volume fraction of each mineral in aggregate, and

E_i = Young's modulus of each mineral phase.

x and $(1 - x)$ = relative proportions of material conforming with the upper and lower bound solutions.

Table 17. Comparative Assessments between Mineral COTE (linear, 10^{-6}/°F) Measured by Dilatometer and Collected from Literature.

Mineral	Dilatometer	ASTM STP 169C (*29*)	Handbook (*28*)
Dolomite	5.34	-	5.22*
Calcite	3.10	2.78	2.81*
Albite	3.62	3.33	3.33*
Anorthite	-	1.67	2.61+
Microcline	3.61	3.61-4.17	2.89+
Quartz	7.22	6.67	-
Magnetite	-	-	3.81+
Pyroxene	-	3.61-4.17	6.73*

*Average of 3 linear COTE along three crystallographic directions (a,b,c) of single crystal; + linear COTE = volume COTE/3

Hirsch's model becomes the series model when $x = 0$, and it becomes the parallel model when $x = 1$. A value of 0.5 is assumed for x and indicates that the chances of occurrence of either parallel or series arrangements of the constituent minerals in the aggregate are equal. The predicted aggregate COTE based on COTE and elastic modulus of pure minerals (Table 16) and their respective calculated mineral volume percent (Table 15) are presented in Table 18. The COTE of all the sampled aggregates were measured by dilatometry and are also listed in the same Table 18 for comparison. Figure 17 shows the graphical representation of measured versus calculated COTE.

Table 18. Mineral Volumes and Calculated COTE for the Tested Aggregates along with Measured COTE by Dilatometer.

Agg-regate	Samp. No.	Mineral Volume (%)								COTE (10^{-6}/°F)	
		Do	Cc	Ab	An	Pf	Qtz	Mt	Pyx	Cal.	Msd.
SRG Method I	1	0.00	2.73	1.91	0.69	1.71	92.25	0.69	0.00	6.88	6.83
	2	0.47	0.06	0.00	1.69	0.85	96.18	0.75	0.00	7.06	7.28
CRG Method I	3	6.71	51.92	0.00	2.44	1.90	35.23	1.79	0.00	4.56	5.11
	4	6.27	67.50	0.00	0.01	1.37	20.87	3.88	0.00	4.02	
Limestone Method I	5	2.37	94.23	0.00	1.17	0.32	1.71	0.19	0.00	3.23	3.53
	6	1.77	97.73	0.09	0.24	0.06	0.07	0.03	0.00	3.15	3.74
	7	2.80	93.29	0.00	0.45	0.41	2.11	0.94	0.00	3.26	3.48
	8	3.92	88.58	0.00	0.44	0.45	5.92	0.68	0.00	3.41	
	9	3.90	89.22	0.46	0.05	0.06	6.26	0.05	0.00	3.42	3.58
	10	7.57	91.96	0.73	0.00	0.13	0.00	0.06	0.00	3.31	
	11	0.68	99.04	0.00	0.00	0.00	0.26	0.02	0.00	3.13	
Sandstone Method I	12	3.56	0.00	12.13	10.46	11.60	58.95	3.31	0.00	5.75	5.72
	13	0.96	0.00	2.66	04.29	3.61	86.93	2.51	0.00	6.69	6.67
Granite, Method II	14	0.00	0.00	32.66	5.31	29.08	24.85	0.00	6.29	4.96	4.89
	15	0.00	0.00	31.48	7.50	25.00	22.33	0.00	11.31	5.16	5.00

Cal. – Calculated, Msd. – Measured; Do – Dolomite, Cc – Calcite, Ab – Albite (Na-feldspar), An – Anorthite, Pf – K-feldspar, Qtz – Quartz, Mt – Magnetite, Pyx – Pyroxene

Perusal of Figure 17 shows that the predicted COTE closely resembles the measured COTE as is evident from higher correlation coefficients ($R^2 = 0.98$) between calculated and measured COTE. Calcareous gravel (impure limestone) deviates slightly from the main trend and shows slightly higher measured COTE (5.11×10^{-6}/°F) than the predicted COTE (4.56×10^{-6}/°F). Additional testing of other calcareous gravels may be needed in order to verify whether this type of aggregate always shows slightly higher COTE measured than predicted COTE.

Aggregate source variability should be reflected in variations in elemental oxide weight percentages if properly sampled. Variation in elemental oxide weight percentages results in mineralogy changes and, hence, changes in COTE (as, for example, the COTE of pure limestone ranges from 3.17×10^{-6}/°F to 3.44×10^{-6}/°F, whereas COTE of impure siliceous limestone ranges from 4.0×10^{-6}/°F to 4.56×10^{-6}/°F). Therefore, the proposed mineralogical modeling is a sensitive tool that could be used for monitoring aggregate source variability relative to aggregate quality control.

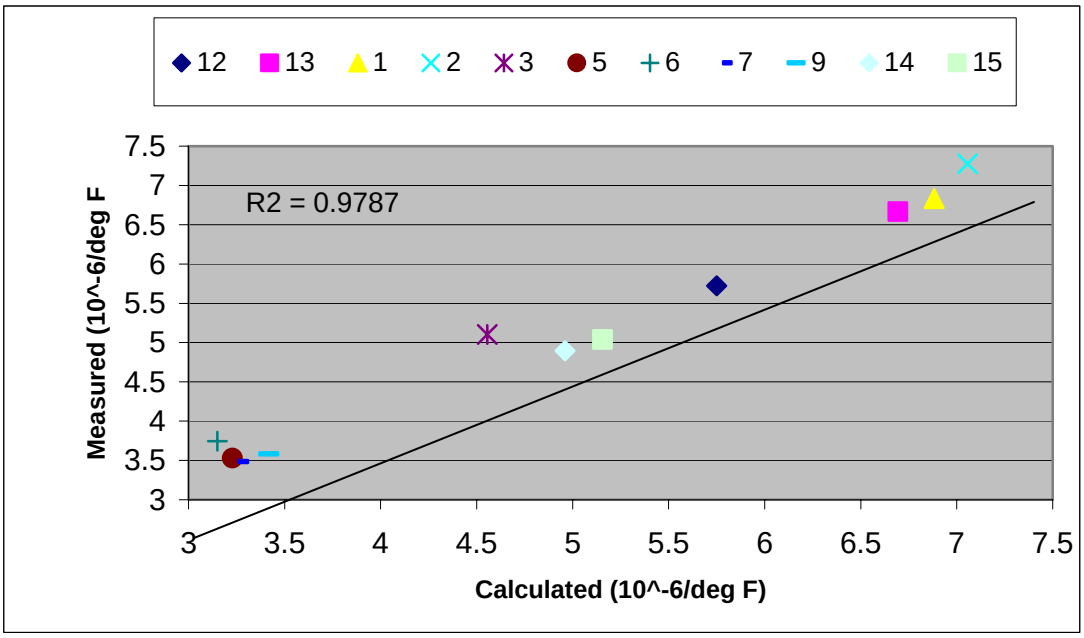

Figure 17. Calculated vs. Measured Aggregate COTE.
(Data Points are Presented in Table 18).

MODELING OF CONCRETE COTE

A computer program, CHEM2, was developed by the Center for Transportation Research, The University of Texas at Austin, Texas, to estimate the chemical properties of concrete from an inexpensive chemical test. The initial versions of the program were developed from a test database containing data from different Texas aggregates. The program requires as input the percentage by weight of certain oxide residues produced by standard fusion testing, for the purposes of predicting concrete f_c' (compressive strength), f_t (splitting tensile strength), E (elastic modulus), and Z (drying shrinkage) for curing times ranging from 1 to 28 days. The program provides a rough approximation of material properties for concrete made with a new aggregate source prior to actual laboratory testing. It also estimates properties for blended aggregates. The methodology of the CHEM2 program is such that it first identifies the type of aggregate and then predicts the performance using a model prepared for that type of aggregate. The program either identifies the aggregate from either the user input or the oxide test results.

CHEM2 is based on regression analysis, and it predicts concrete properties without real input of concrete mixture proportions. This program predicts mineral weight

percent of all types of aggregates based on a common set of chemical formulae (similar to method I). The present study (discussed earlier) has demonstrated the requirements of two different set of formulae (method I and II) to calculate mineral weight percent for all rock types instead of a common set of formulae.

New Approach

The model to predict concrete COTE is based on the concept of Hirsch's composite model (*8, 30*), where determined COTE of mortar and coarse aggregate are the two main inputs. Our proposed concrete COTE model is basically a two-step model (i.e., (i) prediction and validation of aggregate COTE, elaborated in the foregoing discussion, and (ii) prediction of concrete COTE based on calculated COTE of aggregate in the first step [Table 14] and known COTE of standard mortar). Measured concrete COTE by dilatometry validates the concrete COTE model by comparing the predicted value to the measured value. The following formula is adopted based on Hirsch's composite modeling to predict concrete COTE:

$$\alpha_c = X(\alpha_m V_m + \alpha_a V_a) + (1 - X)\frac{\alpha_m V_m E_m + \alpha_a V_a E_a}{V_m E_m + V_a E_a} \qquad (11)$$

where

α_m, α_a = COTE of mortar and aggregate,

V_m, V_a = volume fraction of mortar and aggregate,

E_m, E_a = elastic modulus of mortar and aggregate, and

X = relative proportions of material conforming with the upper and lower bound solution.

The COTE of a standard mortar specimen (8.06×10^{-6}/°F) using the same sand and same sand to cement ratio that was used in the concrete was measured by dilatometry and used as the fixed-mortar COTE input in the concrete COTE model. Volume fractions of mortar and aggregate are calculated from mixture proportions of the tested concrete specimens and are given in Table 19. A value of 1×10^6 psi [6895 MPa] was used as the fixed input for modulus of elasticity (MOE) of mortar. It is observed that

Table 19. Mix Proportions of Concrete Specimens.

Type of Coarse Aggregate	Coarse Aggregate (lb)	Fine Aggregate (lb)	Cement (lb)	Fly Ash (lb)	Water (kg)	Ap. SG (CA)	V_{CA}	V_m
SRG-1	2314.85	1403.33	601.86	258	361	2.62	0.4214	0.5786
SRG-2	2314.85	1386.00	601.86	258	361	2.60	0.4247	0.5753
CRG-3	2314.85	1394.58	601.86	258	361	2.61	0.4230	0.5769
Lst-5	2314.85	1403.33	601.86	258	361	2.62	0.4214	0.5786
Lst-6	2314.85	1403.33	601.86	258	361	2.61	0.4223	0.5776
Lst-9	2314.85	1394.58	601.86	258	361	2.60	0.4240	0.5760
Sst-12	2314.85	1454.54	601.86	258	361	2.67	0.4128	0.5872
Granite-14	2314.85	1437.72	601.86	258	361	2.65	0.4150	0.5850
Granite-15	2314.85	1437.72	601.86	258	361	2.66	0.4150	0.5850

CA – Coarse aggregate, SG – Specific gravity, V_{CA} – Volume fraction of CA, V_m – Volume fraction of mortar, Lst – Limestone, Sst – Sandstone; Type of coarse aggregate is in accordance with Table 13.

(MOE) of mortar. It is observed that MOEs of 5×10^6 to 10×10^6 psi [34474 to 68948 MPa] represent nearly all natural rocks commonly used as aggregates. Researchers have found from modeling of elastic modulus that, at least for some concretes, *X* is approximately 0.5 (*31*). Therefore, 0.5 was assigned for *X* in the present study. Cast concrete specimens (cylindrical 8 × 4 inch [20.3 × 10.2 cm] specimens) were sliced into 4 inch (10.2 cm) diameter × 5.5 inch (14.0 cm) height dimensions after 28 days of moist curing. The COTE of these sliced cylindrical specimens was measured by dilatometer. Predicted and measured concrete COTE are presented in Figure 18. Perusal of Figure 18 indicates that predicted COTE shows good correlation with measured COTE, with a correlation coefficient of around 0.97. The effect of changing aggregate MOE (from 5×10^6 to 10×10^6 psi) on predicted concrete COTE was also checked. It was observed that the predicted concrete COTE slightly decreases with increasing aggregate MOE. It is interesting to note that the correlation coefficient between predicted and measured COTE remains unchanged while changing aggregate MOE. Therefore, a fixed value of the aggregate MOE was set at 8×10^6 psi to simplify the prediction of the concrete COTE. However, one can use the actual elastic modulus of tested aggregate if desired to predict the concrete COTE.

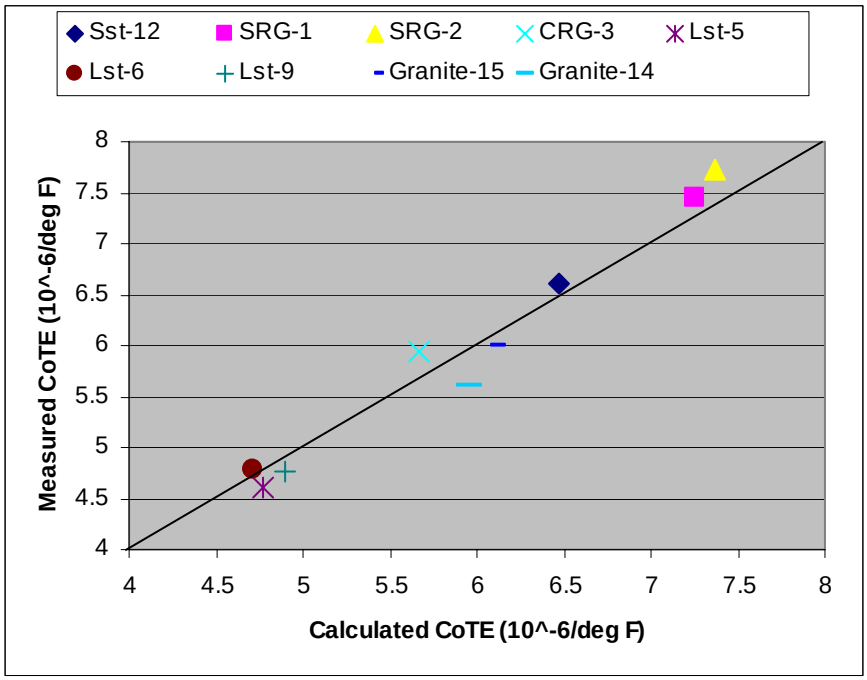

Figure 18. Calculated vs. Measured Concrete COTE. (Mixture Proportions for the Corresponding Concretes are Listed in Table 19).

The developed aggregate and concrete COTE model was applied to estimate the COTE of field concrete. A core sample was obtained from recently paved (July-August 2004) concrete pavement on SH 330 near Baytown, Texas, six months after placement of the concrete. The mixture proportion of the concrete is given in Table 20. COTEs of aggregate and concrete were predicted using the developed model and measured by dilatometry and are presented in Table 21. Table 21 shows that both measured and predicted aggregate and concrete COTE compared well and further validated the applicability of the COTE model for field concrete.

Table 20. Mixture Proportion of Field Concrete Core Tested by Dilatometer.

Materials	Proportions, lb (kg)
Coarse aggregate (limestone)	1695.8 (769.2)
Fine aggregate (siliceous sand)	1413.7 (641.2)
Cement (Type I)	362.2 (164.2)
Fly ash (Class F)	129.1 (58.6)
Water	220.1 (99.8)
w/c Ratio	0.45
Air entrained admixture (AEA)	1.3 (0.59)

Table 21. Measured vs. Predicted Aggregate and Concrete COTE for the Tested Field Concrete.

	COTE (10^{-6}/°F)	
	Predicted	**Measured**
Aggregate	3.26	3.32
Concrete	5.11	5.00
Mixture parameter: V_{mortar} = 0.5987 and $V_{Coarse\ aggregate}$ = 0.4013		

CONCLUSIONS

A new mineralogical approach is presented to predict aggregate and concrete coefficient of thermal expansion based on Hirsch's composite modeling. The following points are drawn as conclusions from the present study:

- The sampling protocol for the aggregate provides a consistent means to select a representative powder sample for bulk chemical analysis. However, more care should be taken in case of highly heterogeneous gravel.
- All three types of rocks (i.e., sedimentary, igneous, and metamorphic) commonly used as aggregates can be considered in the present model by maintaining their separate entity.
- Different aggregates are well represented by the weight percentage of minerals actually present. The calculated mineralogy based on the proposed modeling and actual mineralogy from XRD compare well. This similarity suggests that the

combination of the proposed two methods is capable of calculating representative mineralogy for all types of aggregates.

- Dilatometer COTE measurement of five pure minerals is fundamental to the development of a model for the prediction of aggregate COTE. The more accurate the estimation of a pure mineral's COTE the better will be the prediction of aggregate COTE because individual mineral COTE is the most important input when calculating aggregate COTE.
- Predicted aggregate COTE by mineralogical modeling compares well with the measured aggregate COTE, except for some minor deviation in calcareous gravel. This similarity validates the composite model for prediction of aggregate COTE. However, more research on different types of aggregates is needed to establish this resemblance, and hence, the effectiveness of composite mineralogical modeling to predict aggregate COTE.
- Different aggregates contain different types of minerals, and this is well reflected in the proposed model. This difference in mineralogy gives rise to different COTE. Therefore, present mineralogical modeling is sensitive to categorizing aggregates based on their COTE values.
- Predicted concrete COTE by composite modeling and measured concrete COTE by the dilatometer shows good correlation. This correlation validates the effectiveness of composite modeling to predict concrete COTE. A change of aggregate MOE from 5×10^6 psi to 10×10^6 psi does not result in significant variation in concrete COTE. Therefore, the composite model for prediction of concrete COTE can be applied to concrete containing a wide variety of aggregates with different COTEs and MOEs.
- Composite modeling will be useful as a check of aggregate source variability in terms of quality control measures and improved design and quality control measures of concrete paving.

INTERLABORATORY (TTI AND TXDOT) TESTING PROGRAM

A preliminary interlaboratory testing program using one aggregate and two concrete specimens was conducted to verify the applicability of dilatometer to measure aggregate and concrete COTE.

Concrete Testing (2002-2003)

TxDOT has recently adopted a test procedure (TEX-428-A) to measure concrete COTE. This test is similar to one developed by AASHTO (*24*). A comparative assessment between concrete COTE determined by TEX-428-A and the dilatometer method was conducted. The similarities between TEX-428-A and the dilatometer test methods are (i) saturated test condition because the specimens are submerged under water during testing and (ii) same testing temperature range, i.e., 10°C (50°F) – 50°C (122°F). The main differences between these two test methods are (i) dilatometer measures volume expansion through monitoring the water level displacement by LVDT. Linear expansion is calculated based on the relation, i.e., linear expansion = 1/3 of volume expansion, (ii) TEX-428-A method directly measures the linear expansion through monitoring the length change of the specimen by LVDT attached to it. Two concrete specimens (CSA 1204 TxDOT – gravel as coarse aggregate and CSA 1205 TxDOT – limestone as coarse aggregate) were supplied by TxDOT to conduct this comparative study. The same concrete cylinder was tested by both test methods. The test results (presented in Table 22) show comparable results between these two different test methods.

Table 22. Comparison of Concrete COTE (10^{-6}/°F) Measured by Dilatometer and Tex-428-A Methods.

Type of Concrete	Dilatometer	TEX-428-A
Limestone concrete	4.76, COV = 4.8%	4.89
Siliceous river gravel concrete	6.61, COV = 4.4%	6.75

Aggregate Testing (Jan-July 2006)

It was decided to conduct an interlaboratory dilatometer testing program using one common aggregate (Trinity gravel) in order to verify the applicability of the dilatometer to measure aggregate COTE. This was decided after resubmission (2005) of the project report based on the first review. The research team has done extensive dilatometer testing on the supplied gravel aggregate with the following additional steps in the test procedure

1. Applying additional vacuum at 50°C (122°F) to ensure the most effective de-airing: After applying 45 minutes normal vacuum (Appendix D) at room temperature, the dilatometer was placed in a water bath and heated to 50°C (122°F). The dilatometer was then removed from the water bath and quickly placed in the vacuum system (Appendix D) for an additional 30-45 minutes vacuum saturation.
2. Introducing heating and cooling cycles: Alternate heating (10°C–50°C [50°F–122°F]) and cooling (50°C–10°C [122°F–50°F]) cycles were applied while keeping the float and dilatometer system untouched. All the earlier test results in this report were based on testing three different aggregate samples from the same barrel at one heating cycle (i.e., 10°C to 50°C [50°F to 122°F]).

Detailed information pertaining to test procedure, test results, data analysis, and data comparison and a brief discussion are presented in Appendix F. The percent COV of the test results and interlaboratory COTE comparison are well within permissible limits. Preliminary interlaboratory test results look very promising. Therefore, an implementation program is recommended in order to use dilatometer as a production level device.

CHAPTER 5. EFFECTS OF AGGREGATE GRADATION ON EARLY-AGE PROPERTIES OF CONCRETE

Aggregate grading that yields maximum density and maximum particle interlock is highly desirable for both plain and reinforced concrete. The aggregates are usually selected and combined according to specification, which dictates the overall aggregate gradation. Selection and mixing of the aggregates influence the quality of concrete. Aggregate gradation effects on cracking-related displacement of concrete were investigated in the laboratory using the German cracking frame. Concrete workability was assessed using the slump and drop tests for two different concrete mixtures consisting of gap-graded and dense-graded aggregates. Shrinkage strain, cracking frame strain, and concrete strain were measured and compared to strength gain and creep development. The measured and calculated strains of the different aggregate gradations were compared with each other. Gradation effects on strength and stress development relative to tensile cracking at saw-cut tip were also investigated.

In addition to gradation of aggregates, the water to cementitious (w/cm) material ratio also plays a major role in determining the strength of concrete. This part of the report contains the results of a study performed to evaluate the test data with respect to the effect of aggregate gradation and w/cm on various early-age properties of concrete and strength.

INTRODUCTION

As noted previously, gap-graded aggregates have a lower dry rodded unit weight (DRUW) and larger total volume of voids to be filled with cement mortar than concrete with dense-graded aggregates. Because of the higher mortar content (cement + water + sand) in the mixture, the concrete with gap-graded aggregates may undergo larger volumetric strain due to shrinkage. On the other hand, dense-graded aggregates have larger DRUW and more extensive surface area to make contact with the mortar. A higher w/cm ratio in concrete also causes higher volumetric strain than concrete with a lower w/cm ratio. Accordingly, the strength of dense-graded concrete should exceed the strength of gap-graded concrete.

THE GERMAN CRACKING FRAME

A procedure to monitor gradation effects on the cracking-related strength and strain over time relative to shrinkage strain was conducted in the laboratory using the German cracking frame. The cracking frame (Figure 19) accommodates a 1 m long concrete specimen. The ends of the specimen are configured by dovetails in two steel cross-heads. These cross-heads are connected with two steel bars to restrain longitudinal change in the distance between the crossheads.

Figure 19. Cracking Frame.

Small longitudinal deformations or strains in the steel bars are calibrated to load in order to determine the longitudinal stress applied to the frame (Figure 20). The concrete specimen cross section at the center portion is 5.05 × 5.75 inch (12.83 × 14.6 cm) and at the ends of the dovetails is 5.05 × 12.95 inch (12.83 × 32.9 cm). It is anticipated that the cracking sensitivity of concrete can be examined within a limited geometric range by comparing test results between different concrete mixtures using the cracking frame. The cracking frame has the added advantage of providing a sufficiently large test specimen to allow for a crack inducer and instrumentation to be inserted in the concrete (*32*). The concrete in the cracking frame was notched at mid-span to induce cracking at that location. The use of the crack inducer ensures that the crack will indeed be controlled in the center in the specimen.

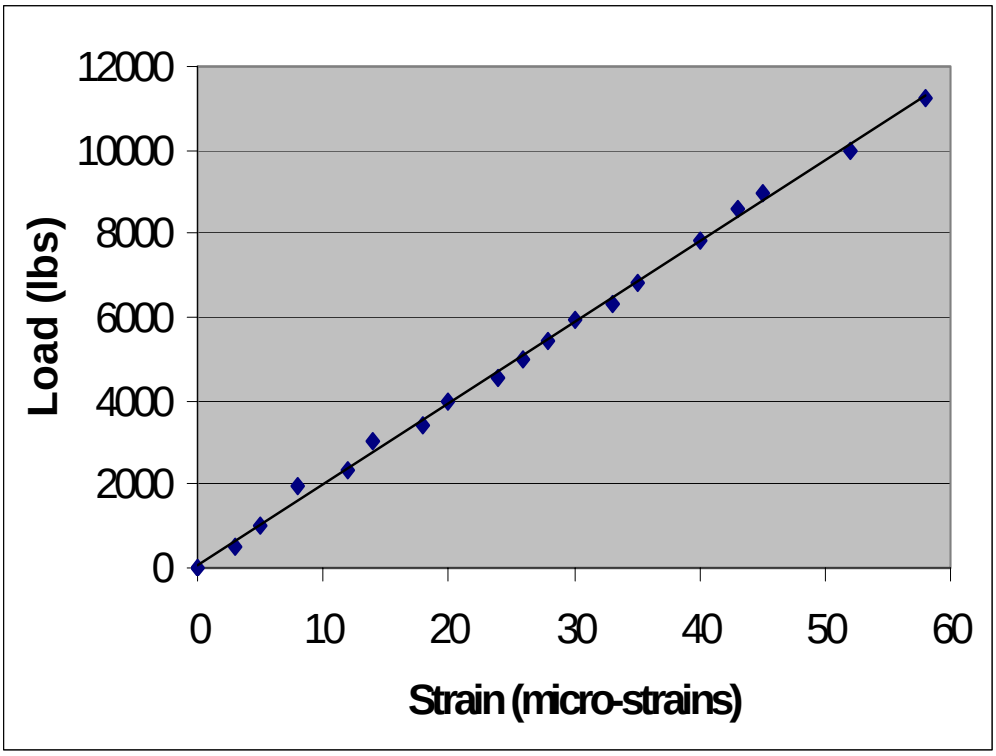

Figure 20. Cracking Frame Force vs. Load Cell Strain.

The cracking frame was instrumented to collect the following data during the hardening process:

- free shrinkage strain (ASTM C 157);
- strain of steel rods;
- concrete strain in the cracking frame;
- concrete temperature (top and bottom);
- concrete compressive strength (1, 3, and 7 days);
- concrete split tensile strength (modified ASTM C 496);
- concrete slump (ASTM C 143); and
- number of drops (a German DIN 1048 test standard).

Demac points were installed on the top surface of ASTM C 157 specimens to measure free shrinkage strain. The specimens were subjected to one-dimensional drying, representative of the drying shrinkage the concrete in the cracking frame is subjected to. The cracking frame strain resulted from restraint of the free shrinkage strain and was

measured by the load cells installed on the steel frame separating the bulkheads. Concrete strain was measured by vibrating wire strain gauges imbedded into the cracking frame concrete. Two thermocouples were also embedded to measure the concrete temperature at 2.54 cm (1 inch) from the top and bottom surfaces. Concrete compressive strength ($f_c^{'}$) was measured in 15.25 × 30.5 cm (6 × 12 inch) standard cylinder specimens to monitor strength gain over time and to provide a basis for determining the degree of hydration and the modulus of elasticity. Concrete split tensile strength was also measured following the modified ASTM C 496 procedure *(33)*. Workability of concrete was measured by the slump test and characterized by the German DIN 1048 drop test method.

LABORATORY TEST PROGRAM

Cracking-related displacements with respect to shrinkage and creep strains were compared using gap-graded and dense-graded aggregates in concrete mixtures as shown in Table 23.

The concrete mixture consisted of crushed limestone as the coarse aggregate, pea gravel as intermediate aggregate (mostly cherty), and natural siliceous sand as the fine aggregate. The coarse aggregate factor (CAF) and intermediate aggregate factor (IAF) were 0.45 and 0.25, respectively, for dense-graded mix. Two cement factors (CF), i.e., 6.0 and 5.0, and two water to cement ratios, i.e., 42 and 0.45, were used.

Concrete Workability

Slump and drop tests were conducted immediately upon mixing the concrete. The drop test (DIN 1048) is a German test standard that measures, to some extent, the mobility of a concrete mixture with a slump less than 50 mm (2 inches) to serve as an indicator of whether workability is sufficient during placement of the concrete. The test is a simple measure of the number of drops taken to cause a concrete mixture in a slump cone to bulge laterally to a given diameter in a consistent and flowable manner. The measured slump and number of drops for each mixture are shown in Table 24. The number of drops of the concrete mixed with dense-graded aggregates is greater than that of open-graded aggregates, although they had the same slump. The concrete mixed with

dense-graded aggregates showed greater resistance to lateral movement. Apparently, the higher adhesion between aggregates and cement mortar of dense-gradation concrete hindered the concrete from bulging laterally.

Table 23. Mixture Proportions in 1 yard^3 (27 ft^3) [0.7646 m^3] of Cracking Frame Concrete.

	Test 1 (G.G.)	Test 2 (D.G.)	Test 4 (G.G.)	Test 5 (G.G.)	Test7 (D.G.)
Cement (lb [kg])	423 (192)	423 (192)	423 (192)	423 (192)	352.5 (160)
Fly ash (lb [kg])	141 (64)	141 (64)	141 (64)	141 (64)	117.5 (53)
Coarse aggregate (lb [kg])	1853.9 (841)	1191.8 (541)	1853.9 (841)	1853.9 (841)	1184.1 (537)
Intermediate aggregate (lb [kg])	-	713.5 (324)	-	-	713.5 (324)
Fine aggregate (lb [kg])	1141 (518)	1114 (505)	1141 (518)	1096.4 (497)	1304.2 (592)
Water (lb [kg])	236.9 (108)	236.9 (108)	236.9 (108)	253.8 (115)	197.4 (90)
Air entraining agent (mL)	180.5	180.5	180.5	180.5	150.4
w/cm	0.42	0.42	0.42	0.45	0.42
CAF	0.7	0.45	0.7	0.7	0.45
IAF	-	0.25	-	-	0.25
CF	6	6	6	6	5
Unit weight (lb/yd^3)	3795.7	3812.6	3795.7	3768	3869.2
Test condition	Ambient	Ambient	40°C 25% Rh	25°C 50% Rh	40°C 25% Rh

G.G. = Gap graded D.G. = Dense graded

Table 24. Slump and Drop Test Results.

	Test 1	Test 2	Test 4	Test 5	Test 7
Slump (mm [in])	40 (1.57)	40	45 (1.77)	180 (7.09)	15 (0.6)
Drop (number)	6	12	6 (broken)	NA	9

Shrinkage and Creep Strains

During the cracking test, the concrete free shrinkage (ASTM C 157) was monitored over time (Figure 21) along with the strain in the concrete and the steel frame. These trends are shown in Figures 21, 22, 23, and 24, respectively. Shrinkage for test 7 was found to be lowest (Figure 22) in the first 70 hours after preparing the concrete. Test 4 on gap-graded aggregate had higher shrinkage than the test 7 on dense-graded aggregate, and shrinkage measured in test 5 was the highest. The strain measured by the concrete gage represents the net effect of shrinkage and elastic strain due to the restraint imposed by the cracking frame; if the strain in the steel frame was zero, the strain measured by this gage would represent the creep strain in the concrete. Otherwise, the difference between the strain measured by the gage in the concrete and strain measured by the gage on the steel represents the creep strain in the concrete. It is noted that the initial portion of the strain shown in Figure 23 should not exceed the amount of free shrinkage measured from the ASTM C 157 specimen, but since it was, this portion was not considered in the creep strain calculation shown in Figures 25 and 26. As previously noted, the cracking frame strain (Figure 24) was measured in the laboratory during the testing sequence, but the load on the concrete (F_s) due to the drying shrinkage was determined using a calibration curve (Figure 20) developed from load cell reading correlated to the strain gauge readings. Free shrinkage strain (Figure 21) was found from ASTM C 157 specimen data, as previously described. The shrinkage strain and the frame strain varied with time, as did the force in concrete. The frame strain was nearly zero until around 40 hours of concrete age. So, a significant amount of creep strain took place over 40 hours.

Analysis of the restraint provided in the cracking frame suggests that the creep strain can be found from the following relation (*32*):

$$\varepsilon_{crp} = \varepsilon_v - \varepsilon_e - \left(\frac{F_s}{E_c A_c}\right) = \varepsilon_{conc} - \varepsilon_e \qquad (12)$$

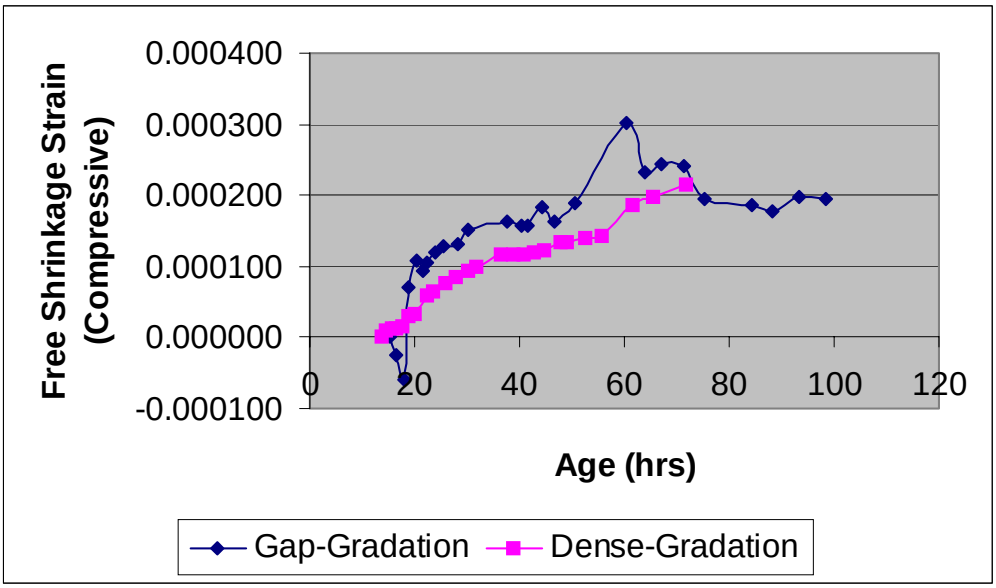

Figure 21. Free Shrinkage Strain vs. Time (Test 1 and Test 2).

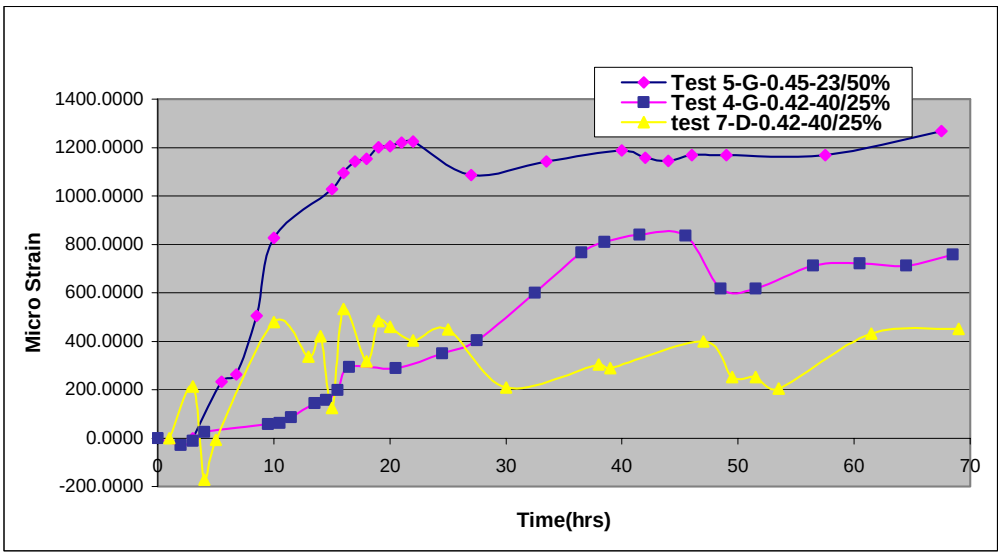

Figure 22. Time vs. Free Measured Shrinkage at Surface.

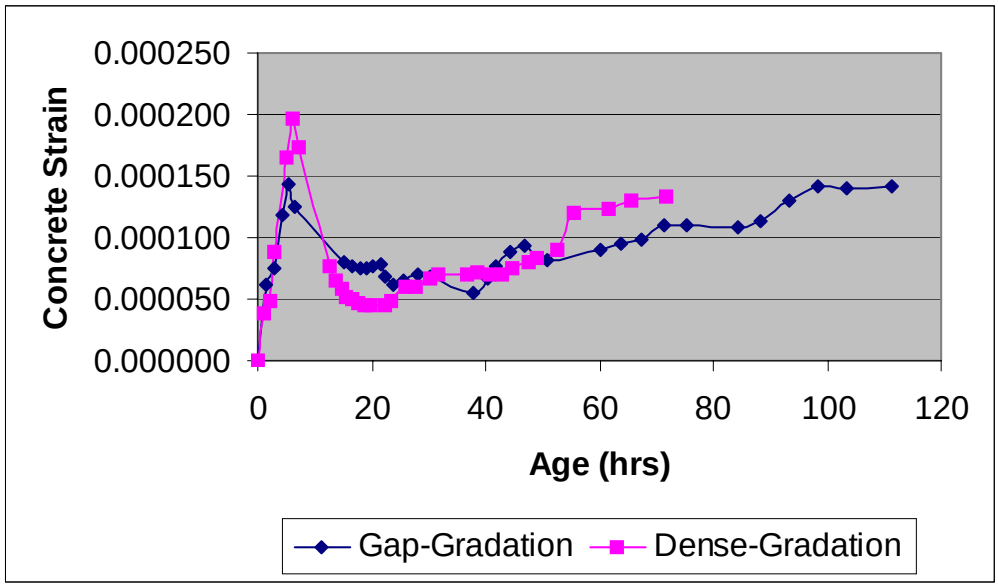

Figure 23. Concrete Strain (Test 1 and Test 2).

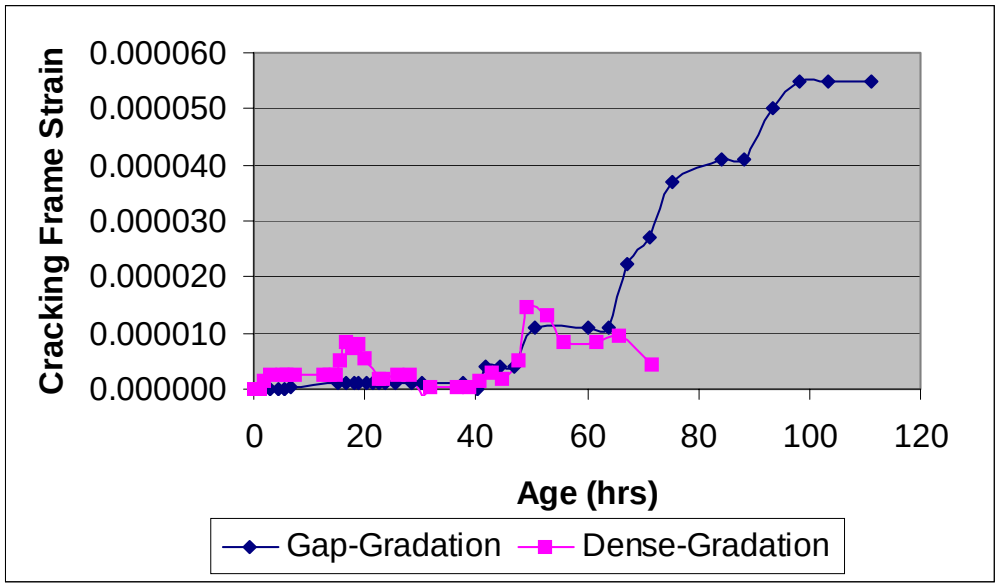

Figure 24. Cracking Frame Strain (Test 1 and Test 2).

where

ε_{crp} = creep strain,

ε_v = shrinkage strain (ASTM C 157),

ε_e = frame strain,

F_s = force in concrete (F),

E_c = modulus of elasticity of concrete (F/L^{-2}), and

A_c = specimen cross-sectional area (L^2).

The accumulative creep curves determined by equation (12) are shown in Figure 25. The total creep strain of concrete mixed with gap-graded aggregates appears to be larger than the dense-gradation concrete. The accumulative creep curves determined by net difference between concrete strain and cracking frame strain with time are shown in Figure 26.

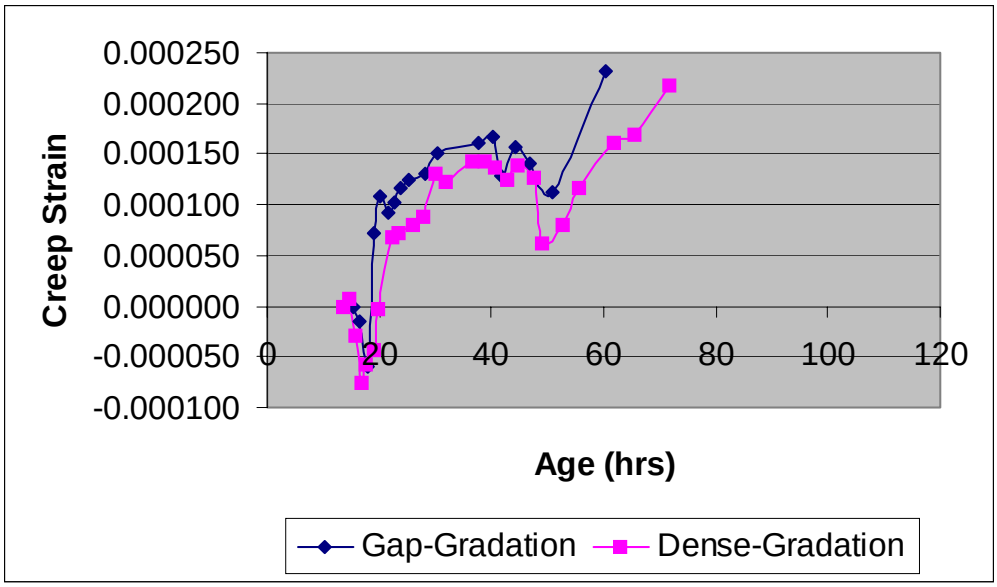

Figure 25. Creep Strain Calculated by Equation (12) (Test 1 and Test 2).

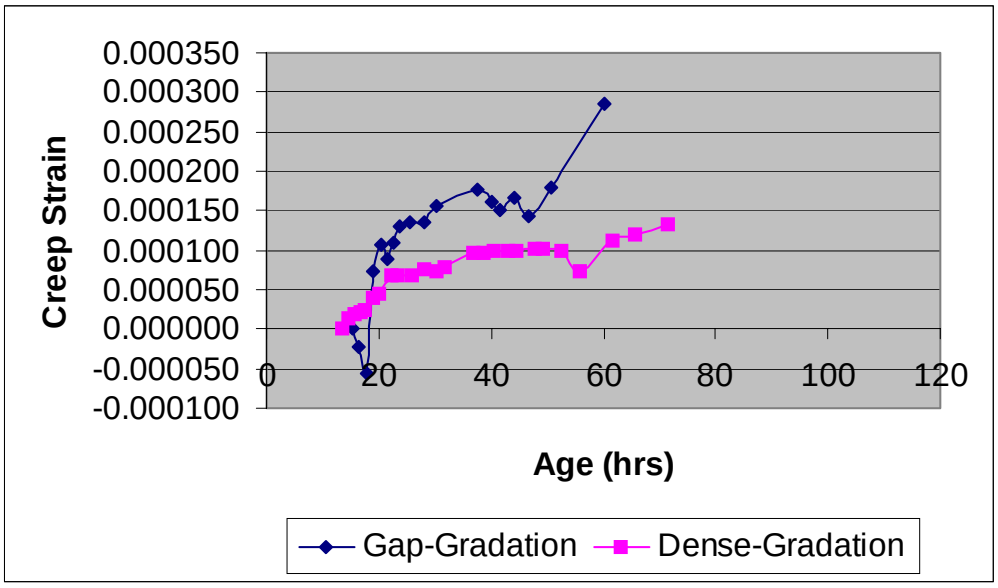

Figure 26. Net Difference between Concrete Strain and Cracking Frame Strain (Test 1 and Test 2).

Cracking at the Notch

The crack formed in the dense-gradation concrete at 69 hours. The time of crack formation of concrete mixed with gap-graded aggregate was not accurately observed. The time of cracking was estimated to be between 55 and 65 hours. The cracks ran through the full depth of the test specimen. The laboratory strength gain with time for both gradations can be seen in Figure 27.

To determine the strength development of the concrete over time, compressive strength tests were conducted at 1, 3, and 7 days. Using specially prepared fracture specimens and following a modified ASTM C 496 procedure (*33*), the fracture parameters (K_{If} and c_f) of the concrete were found and used to determine the cracking strength over time based on the use of fracture mechanics. The tensile strength (f_t) at the tip of the notch was determined using the following equation:

$$f_t = \frac{K_{If} c_n}{\sqrt{g'(\alpha) c_f + g(\alpha) h}} \qquad (13)$$

where

$g'(\alpha)$ and $g(\alpha)$ = slab geometry factors,

K_{If} = stress intensity factor ($F/L^{-2}\ L^{-1/2}$),

c_f = process zone length (L),

c_n = arbitrarily defined constant, and

h = slab thickness (L).

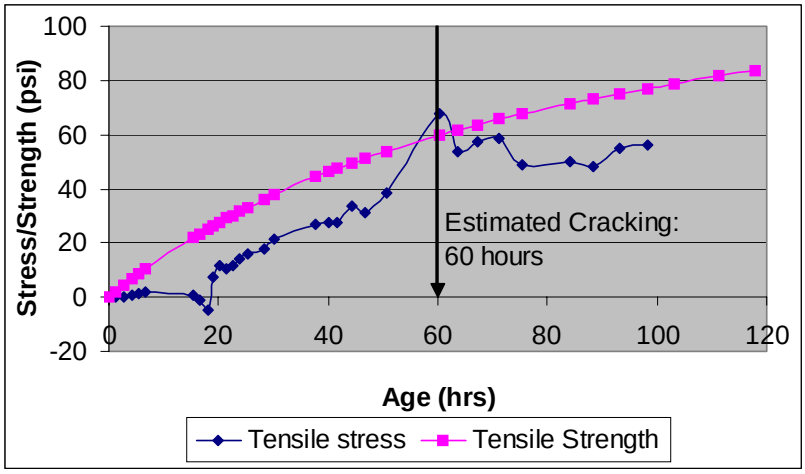

(a) Gap-Gradation

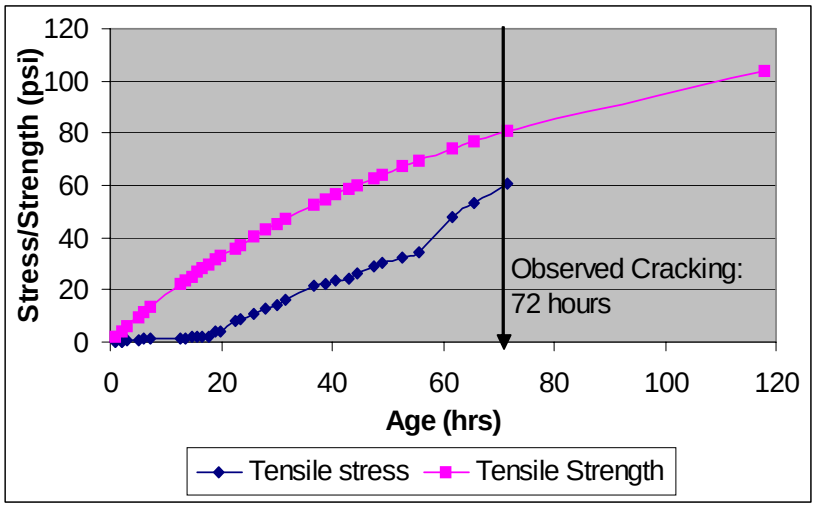

(b) Dense-Gradation

Figure 27. Stress and Strength Development (Test 1 and Test 2).

Tensile stress of the concrete was calculated based on the restraint of shrinkage and thermal strains. Comparing to gap-gradation concrete, higher tensile strength and lower tensile stress were developed in the concrete specimen mixed with dense-graded aggregates as shown in Figure 27. The estimated time of cracking of gap-gradation concrete coincides with the calculated cracking time as shown in Figure 27(a). However, the calculated tensile stress of dense-gradation concrete did not exceed the concrete strength at the time of the observed cracking (Figure 27(b)). The observed time of cracking at the notch was 96, 90, and 108 hours after placement for test runs 4, 5, and 7 respectively.

Compressive Strength

The effect of aggregate gradation on compressive strength of concrete was analyzed. The cylindrical specimens were tested at four different ages to find the compressive strength of the concrete using a standard ASTM procedure. The compressive strength development of test runs 1 and 2 was compared and is presented in Figure 28.

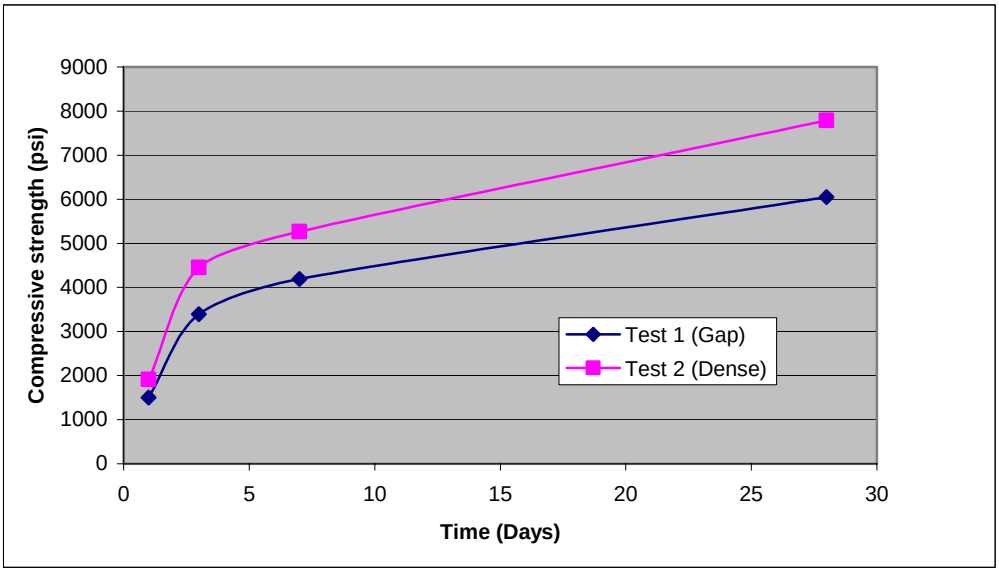

Figure 28. Compressive Strength Results.

CONCLUSIONS

The concrete mixed with gap-graded aggregates had CAF = 0.7, whereas the concrete with dense-graded aggregate had CAF = 0.5 and IAF = 0.25. The gap-graded concrete has larger shrinkage and creep strains than dense-gradation concrete, perhaps because of the higher volume content of cement mortar in the mixture. Because of the larger shrinkage strain, higher restraint tensile stress was developed in the gap-gradation concrete. Lower levels of tensile strength were developed in gap-gradation concrete due to its higher cement content and more extensive surface area of aggregates to contact the mortar. As a result, a crack formed in the concrete mixed with gap-graded aggregates earlier than in the concrete mixed with dense-graded aggregates. Tests with low cement factors showed lower shrinkage, but even then the compressive strengths of the dense-graded specimens were higher than those in the concrete prepared with gap-graded aggregate.

CHAPTER 6. SUMMARY AND FOLLOWUP FOR IMPLEMENTATION

This report discusses the modified test method (dilatometer) to measure aggregate and concrete COTE. The new approach to predicting the aggregate and concrete COTE based on the mineralogy of the aggregate and the mix proportions of the concrete is also well documented. In addition, the investigated effects of gradation on early-age properties of concrete are detailed. In terms of implementation, a follow-up report will address the following topics:

- key COTE design issues,
- assessment of aggregate and concrete COTE variance,
- assessment of aggregate and concrete COTE sensitivity,
- aggregate and concrete COTE implications and significance on design,
- effects of aggregate blending on COTE, and
- characterization of COTE for design purposes.

Under a change in temperature, an unrestrained material will change shape proportional to the amount of temperature change multiplied by its COTE. The COTE indicates how much material shape will change for each degree of temperature change. The COTE is, therefore, a fundamental engineering property that quantifies the change in unit length per degree of temperature change.

As aggregates themselves comprise of a variety of minerals, it has been shown that their COTE varies with mineralogical composition and porosity. Quartz has the highest COTE of any common mineral, and aggregates with high quartz content have high COTE values. The COTE of hardened concrete is variable, depending on the mixture design and the type of aggregate used. Since aggregates make up the bulk of concrete, their properties will largely determine concrete's COTE. With a known mixture proportion, the COTE of hardened concrete can be roughly estimated from a weighted average of all its components.

The overall strategy to implement the measurement and specification of COTE is shown in Figure 29 and is divided into two main sections: quality control and quality assurance.

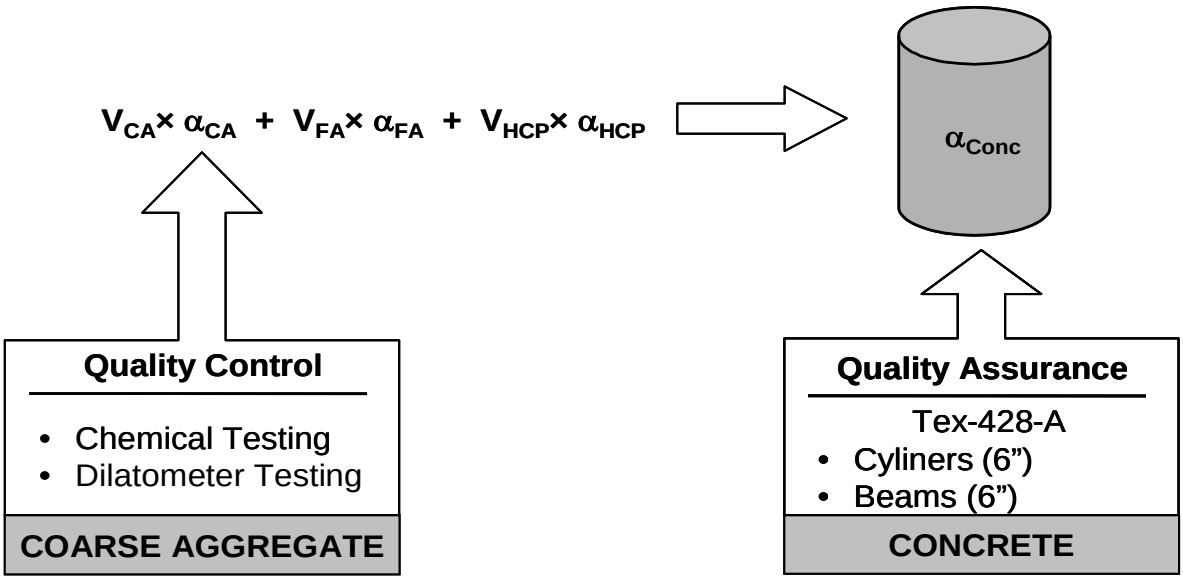

Figure 29. Schematic of Overall CoTE Implementation Strategy.

QUALITY CONTROL (QC) TESTING ON THE AGGREGATE SOURCE

In concept, coarse aggregates taken from various sources can be sampled at specified intervals. After calculating the mineral composition from bulk chemical analysis of the aggregates, the COTE of coarse aggregates (α_{CA}) can be predicted from mineralogical modeling. COTE can also be directly measured by dilatometer testing. The aggregate coefficient of expansion (α_{CA}) is used along with the concrete mixture proportions to calculate the COTE of the concrete. As shown in Figure 29, the COTE of the concrete mixture (α_{Conc}) is then estimated based on a weighted average of all the mixture components, which include the coarse aggregate, fine aggregate, and hydrated cement paste.

QUALITY ASSURANCE (QA) TESTING ON THE CONCRETE

During construction, QA testing on the concrete will be performed at specified intervals. The specimens for this test will involve either the concrete as delivered to site (cylinders or beams) or the concrete as placed (cores). Long-term pavement performance is related to the in situ COTE value achieved, and enforcement could, therefore, eventually be based the percentage of design life that will result due to the COTE as constructed.

TESTING PROCEDURES

Three test procedures related to work from Project 0-1700 are pertinent for further consideration relative to implementation. Brief discussions of each are presented below.

Chemical Analysis of Coarse Aggregates

The CHEM 2 program previously described (Chapter 4) was developed to estimate the concrete COTE based on the mineral composition of the coarse aggregate. This procedure allows calculation of concrete COTE values knowing the mixture proportion of the concrete and the aggregate mineralogy. The process requires sampling of coarse aggregates and a chemical analysis of a representative powdered sample. Once the chemical composition of the aggregates has been determined, the concrete COTE can be estimated.

Dilatometer

The dilatometer was recently developed at TTI to estimate the COTE of aggregates. The dilatometer determines the COTE of the aggregate by measuring the volumetric expansion after a controlled temperature increase. The dilatometer can also be used to determine the COTE of concrete.

TxDOT Test Tex-428-A

TxDOT recently documented a test procedure (Tex-428-A) to determine the COTE of a concrete sample. This test is similar to one developed by AASHTO. The procedure requires a 4 inch core, cut to a length of 7 inches. The sample is saturated for

more than 48 hours and then subjected to a temperature change of 40°C (104°F) in a water bath. The length change of the specimen is measured and, with the known length change of the measuring apparatus under the same temperature change, the COTE of the concrete specimen can be determined.

SPECIFICATION DEVELOPMENT

Development of a draft specification (Appendix G) will provide guidelines for COTE that ensure that design conditions are achieved during construction. The variability of aggregates and concrete COTE values need to be addressed as part of the specification as well as aggregate prequalification, quality control testing, and quality assurance testing during actual construction.

Quality Control Testing

The COTE implementation approach for the QC and QA testing phases were previously shown in Figure 29. Quality control testing on the raw aggregate sources would eliminate the need for concrete samples. Quality control testing can either be based on chemical testing of the aggregate mineralogy or on dilatometer results. The required sampling procedure and frequency of testing are explained in Chapter 4.

Quality Assurance Testing

Quality assurance testing should be performed on the hardened concrete. This is necessary to validate that the COTE of the concrete as constructed meets the COTE assumed during design. Either the dilatometer or TxDOT test Tex-428-A is recommended to determine the COTE of concrete specimens. Ideally, the COTE from samples cored out of the pavement should be tested, but it can also be determined from molded specimens collected on site. Six inch cylinders can be used for this purpose, but this would require that additional COTE specimens be made. The other possibility is that 6 inch beams, commonly used for strength testing, be used for quality assurance testing. The frequency of quality assurance testing will also be addressed in the specifications.

CLASSIFICATION OF AGGREGATES BASED ON TEXTURE AND COTE

The classification of the coarse aggregate can be done in a format of Tα-N where:

- **T** represents the measure of aggregate texture that ranges from 0 to 1200, e.g., L - low texture, M – medium texture, and H – high texture.
- α represents the measured COTE of the aggregate in whole number of micro strain/°F with a range of 2.78 to 6.66 micro strain /°F, e.g., L – low, M - medium, and H – high.
- **N** represents name of the aggregate, e.g., siliceous river gravel (SRG), calcareous river gravel (CRG), limestone (LST), sandstone (SST), and granite (GRN).

A perusal of Table 25 below illustrates the aggregate classification system in the above Tα-N format.

Table 25. Aggregate Classification System in Tα-N Format.

Texture (T)	COTE (α)	Aggregate name (N)	Classification in Tα -N format
Low texture (L)	High (H)	SRG-uncrushed	LH-SRGUC; UC - uncrushed
Low texture (L)	High (H)	SRG-crushed (e.g., chert dominated gravel)	LH-SRGC; C - crushed
Medium texture (M)	High(H)	SRG-crushed (quartzite dominated gravel)	MH-SRGC
Medium texture (M)	Low (L)	Limestone – LST	ML-LST
Low texture (L)	Low (L)	Limestone – LST	LL-LST
Medium texture (M)	Medium (M)	Siliceous limestone – SLST	MM-SLST
Medium texture (M)	Low (L)	Marble (MRB)	ML-MRB

Aggregate COTE is classified in three categories based on its affect on concrete pavements. Low COTE value of aggregate is desired for better performance of pavements.

Texture values which have five different categories are shown in Table 6 in Chapter 2. High roughness (i.e., high texture index of aggregate) enhances the mechanical bonding and concrete performs well.

A comprehensive aggregate classification system based on relevant physical and chemical properties of aggregate will be the more realistic approach in order to make the concrete pavement resistant to all possible distress. Table 26 can be considered as an example of comprehensive aggregate classification system. It is anticipated that COTE, surface free energy (SFE), and activation energy (with respect to alkali-silica reaction) will be the prime factors to categorize the aggregates in a scale of performance. However, it demands a comprehensive database on SFE and activation energy (E_a) of all commonly used aggregate in Texas to establish this kind of comprehensive aggregate classification system. It also demands to establish the effect of aggregate SFE and E_a on pavement performance. Therefore, further research is required to make this type of aggregate classification system feasible.

Table 26. A Comprehensive Aggregate Classification System.

Aggregates	Minerals (major)	Mineral wt%	Moh's Hardness	COTE (10^{-6}/°F)	Texture index	Surface free energy	ASR reactivity (E_a)
Pure limestone	Cc	Cc – 90-100	3	2.8-3.6		H	NR
Siliceous limestone	Cc + Qtz ± Flsp	Cc – 80-90 Qtz – 10-05 Flsp – 0-5	4	3.8-5.0		H	NR-R
Siliceous river gravel	Qtz ± Chdny ± Opal	Qtz – 60-70 Chdny–20-30, Opal – 0-20	7	6.0-7.2	200	L	PR-R
Heterogeneous river gravel (siliceous rocks + some other type of rocks)	Qtz ± Chdny ± Opal ± Cc ± Flsp ± Bt ± Amph ± Hem/Mt		5-6	5.0-6.5		L-M	PR-R
Calcareous river gravel	Cc ± Qtz ± Chdny ± Opal ± others		4-5	4.0-5.2		M-H	NR-R (depending on type of silica minerals)
Granite	Qtz ± Flsp ± Bt ± Amph ± Apt ± Hem/Mt		6-7	4.4-5.5		M	NR
Sandstone	Qtz ± Flsp ± Cc ± Hem/Mt ± Chl ± Amph		5-6	5-7.5		L-M	NR-PR

Cc = calcite, Qtz = quartz, Flsp = feldspar, Chdny = chalcedony, Bt = biotite, Amph = amphibole, Hem = hematite, Mt = magnetite, Apt = apatite, Chl = chlorite.

REFERENCES

1. McCullough, B.F., Zollinger, D.G., and Dossey, T., "Evaluation of the Performance of Pavements Made with Different Coarse Aggregate," Research Report 3925-1F, Center for Transportation Research, The University of Texas at Austin, Austin, Texas, September 1998.

2. Mitchell, L.J., "Thermal Expansion Tests on Aggregates, Neat Cements, and Concrete," *ACI Journal,* Vol. 48, June 1953, pp 964-977.

3. Meyers, S.L., "How Temperature and Moisture Changes May Affect Durability of Concrete," *Rock Products*, Vol. 54, No. 8, August 1951, pp 153-162.

4. Neville, A.M., *Properties of Concrete*, John Wiley and Sons, New York, New York, 1997.

5. Huang, Y.H., *Pavement Analysis and Design*, Prentice Hall, Englewood Cliffs, New Jersey, 1993.

6. Davis, R.E., "A Summary of the Results of Investigations Having To Do with Volumetric Changes in Cements, Mortars and Concrete, Due to Causes Other Than Stress," *ACI Journal*, Proceedings, June 1930, pp 407-443.

7. Mullen, W.G., Bloem, D.L., and Walker, S., "Effects of Temperature Changes on Concrete As Influenced by Aggregates," *ACI Journal*, Vol. 48, April 1952, pp 661-679.

8. Hirsch, T.J., "Modulus of Elasticity of Concrete Affected by Elastic Moduli of Cement Paste Matrix and Aggregate," *ACI Journal*, Vol. 59, No. 3, March 1962, pp 427-451.

9. Kaplan, M.F., "Flexural and Compressive Strength of Concrete as Affected by the Properties of Coarse Aggregates," *ACI Materials Journal*, American Concrete Institute, Vol. 55, 1959, pp 1193-1208.

10. Peapully, S., Zollinger, D.G., and McCullough, B.F., "Procedure for Classification of Coarse Aggregate Based on Properties Affecting Performance," Research Report 1244-9, Texas Transportation Institute, The Texas A&M University System, College Station, Texas, November 1994.

11. Masad, E., "The Development of a Computer Controlled Image Analysis System for Measuring Aggregate Shape Properties," NCHRP-IDEA Project 77 Final Report, Transportation Research Board, National Research Council, Washington, D.C., 2003.

12. Fletcher, T., Chandan, C., Masad, E., and Sivakumar, K., "Aggregate Imaging System (AIMS) for Characterizing the Shape of Fine and Coarse Aggregates," Transportation Research Board, National Research Council, Washington, D.C., 2003, CD-ROM.

13. Wang, L., and Zollinger, D.G., "A Mechanistic Design Framework for Spalling Distress," Transportation Research Record, *Journal of the Transportation Research Board,* No. 1730, Washington, D.C., 2000, pp 18-24.

14. Senadheera, S.P., and Zollinger, D.G., "A Framework for Incorporation of Spalling in the Design of Concrete Pavements," *Transportation Research Record 1449,* Transportation Research Board, National Research Council, Washington D.C., 1994.

15. Senadheera, S., and Zollinger, D.G., "Influence of Coarse Aggregate in Portland Cement Concrete on Spalling of Concrete Pavements," Research Report 1244-11, Texas Transportation Institute, The Texas A&M University System, College Station, Texas, October 1996.

16. Brown, R.D., "Thermal Movement of Concrete," Current Practice Sheet, No. 3PC/06/01, Cement and Concrete Association, Waxham Springs, Slough, England, November 1972.

17. Won, M., Hankins, K., and McCullough, B.F., "Mechanistic Analysis of Continuously Reinforced Concrete Pavements Considering Material Characteristics, Variability, and Fatigue," Report No. 1169-2, Center for Transportation Research, University of Texas at Austin, Austin, Texas, April 1990.

18. Willis, T.F., and DeReus, M.E., "Thermal Volume Change and Elasticity of Aggregates and Their Effect on Concrete," *Proceedings, American Society for Testing and Materials,* Vol. 39, 1939, pp 919.

19. U.S. Army Corps of Engineers, *Handbook for Concrete and Cement*, Complete Edition, Waterways Experiment Station, Vicksburg, Mississippi, August 1949.

20. Venecanin, S.D., "Thermal Incompatibility of Concrete Components and Thermal Properties of Carbonate Rocks," *ACI Materials Journal*, Vol. 87, No. 6, 1990, pp 602-607.

21. Mitchell, L.J., "Thermal Expansion Test on Aggregate, Neat Cement and Concrete," Proceedings, *American Society for Testing and Materials*, Vol. 53, 1953. pp 963-975.

22. Verbeck, G.J., and Hass, W.E., "Dilatometer Method for Determination of Thermal Efficient of Expansion of Fine and Coarse Aggregate," Highway Research Board, Proceedings of the Thirtieth Annual Meeting, Jan. 9-12, 1951, Washington, D.C., p 187.

23. Gnomix pvT High Pressure Dilatometer. http://www.datapointlabs.com/ExpCapShowDetails.asp?InstId=10 accessed 4 September 2004.

24. AASHTO TP 60-00, "Standard Test Method for the Coefficient of Thermal Expansion of Hydraulic Cement Concrete" – the standard as written was based on the procedures and equipment developed by the FHWA TFHRC to test the CTE of cores taken for many PCC pavements in the long term pavement performance program (LTPP), Washington, D.C., January 2000.

25. Shon, C.S., Lim, S., Mukhopadhyay, A.K., Zollinger, D.G., and Sarkar, S.L., "New Aggregate Characterization Tests for Thermal and ASR Reactivity Properties," Proceedings, ICAR 10th Annual Symposium, Baltimore, Maryland, April 2002.

26. Mukhopadhyay, A.K., Zollinger, D.G., and Sarkar, S.L., "New Mineralogical Approach to Predict Aggregate Coefficient of Thermal Expansion (COTE) Based on Dilatometer and Bulk Chemical Analysis," Proceedings, ICAR 11th Annual Symposium, Austin, Texas, April 2003.

27. *Handbook of Chemistry and Physics*, 71st Ed., CRC Press, Boca Raton, Florida, 1990-1991.

28. Ahrens, T.J., *Mineral Physics and Crystallography*, A Handbook of Physics Constants, AGU Reference Shelf 2, Washington, D.C., 1995.

29. Klieger, P., and Lamond, J.F., "Significance of Tests and Properties of Concrete and Concrete-Making Materials," American Society for Testing and Materials, In: D.S. Lane, Thermal Properties of Aggregates, ASTM STP 169C, Philadelphia, 04-169030-07, 1994, pp 438-445.

30. Zollinger, D.G., Tang, T., Fowler, D., and Wang, L., "Development of a Test Apparatus to Measure Thermal Expansion of Concrete Aggregates," Interim Research Report (2992-1), Texas Transportation Institute, Texas A&M University System, College Station, Texas, 1998.

31. Mindess, S., and Young, J.F., *Concrete*, Prentice Hall, Inc., Englewood Cliffs, New Jersey, 1981.

32. Vepakomma, S., Jeong, J.H., and Zollinger, D.G., "Characterization of Cracking Restraint at Saw-Cut Joints Using the German Cracking Frame," *Transportation Research Record 1813*, Transportation Research Board, National Research Council, Washington D.C., 2002.

33. Tang, T., Yang, S.C., and Zollinger, D.G., "Determination of Fracture Energy and Process Zone Length Using Variable-Notch One-Size Specimens," *ACI Materials Journal*, Vol. 96, No. 1, Jan.-Feb. 1999, pp 3-10.

APPENDIX A

RELATIONSHIP BETWEEN THE COEFFICIENT OF LINEAR THERMAL EXPANSION AND THE COEFFICIENT OF VOLUMETRIC THERMAL EXPANSION

The coefficient of linear thermal expansion and the coefficient of volumetric thermal expansion are designated by α and γ, respectively. When the temperature increases by ΔT, the volume of a body expands from V_1 to V_2. Any length within the body expands from L_1 to L_2. The coefficients α and γ are defined as follows:

$$L_2 = L_1 \times (1+ \alpha\Delta T)$$

$$V_2 = V_1 \times (1+ \gamma\Delta T)$$

The relationship between α and γ is:

$$\gamma = 3\alpha$$

This relationship holds for a body of any regular and irregular shapes. The relationships for the cylinder and for any irregular shape are verified as follows.

CYLINDER

The volume of a cylinder with radius of r and height of h is:

$$V_1 = \pi r^2 h$$

After thermal expansion, the radius becomes r (1 + $\alpha\Delta T$) and the height becomes h (1 + $\alpha\Delta T$), therefore, the volume of the cylinder becomes:

$$
\begin{aligned}
V_2 &= \pi r^2 (1+\alpha\Delta T)^2 h (1+\alpha\Delta T) \\
&= \pi r^2 h (1+\alpha\Delta T)^3 \\
&= \pi r^2 h (1+\alpha^3\Delta T^3 + 3\alpha\Delta T + 3\alpha^2\Delta T^2) \\
\gamma &= \frac{V_2 - V_1}{V_1 \Delta T} = \alpha^3\Delta T^2 + 3\alpha + 3\alpha^2\Delta T
\end{aligned}
$$

Since $3\alpha^2\Delta T$ and $\alpha^3\Delta T^2$ are much smaller than 3α, they can be neglected, and the above equation becomes:

$$\gamma = 3\alpha$$

IRREGULAR SHAPE

For an irregular shape, the volume of a body can be obtained by summing up all the infinitesimal cubics, that is, triple integral:

$$
\begin{aligned}
V_1 &= \iiint_{\Omega} dV = \iiint_{\Omega} dxdydz \\
V_1 &= V
\end{aligned}
$$

Where Ω defines the boundary of the volume. After thermal expansion, the length element dx becomes $(1 + \alpha\Delta T)dx$, dy becomes $(1 + \alpha\Delta T)dy$, dz becomes $(1 + \alpha\Delta T)dz$, and then the volume element dV becomes $(1 + \alpha\Delta T)^3 dV$. Therefore, the volume of the body becomes:

$$
\begin{aligned}
V_2 &= \iiint_{\Omega} (1+\alpha\Delta T)^3 dV \\
&= (1+\alpha\Delta T)^3 \iiint_{\Omega} dV \\
&= (1+\alpha\Delta T)^3 V
\end{aligned}
$$

Where since $(1 + \alpha\Delta T)^3$ is a constant, it is moved out of the integral. Therefore, the volumetric coefficient of thermal expansion is:

$$\gamma = \frac{V_2 - V_1}{V_1 \Delta T} = \alpha^3 \Delta T^2 + 3\alpha + 3\alpha^2 \Delta T$$

Since, α is a small quantity, $3\alpha^2 \Delta T$ and $\alpha^3(\Delta T)^2$ are much smaller than 3α. For example, with $\alpha = 6 \times 10^{-6}$ /°C and $\Delta T = 10$ °C, $3\alpha = 1.8 \times 10^{-5}$ /°C, while $3\alpha^2 \Delta T = 1.08 \times 10^{-9}$ /°C and $\alpha^3(\Delta T)^2 = 2.16 \times 10^{-14}$/°C. Therefore, $3\alpha^2 \Delta T$ and $\alpha^3(\Delta T)^2$ can be neglected in the above equation, and the volumetric and linear coefficients of thermal expansion, γ and α, have the following precise relation:

$$\gamma = 3\alpha$$

This relation is valid for a body of any shape.

APPENDIX B

CALIBRATION PROTOCOL FOR THE DILATOMETER

Following are the guidelines for calibration of dilatometer.

1. Run the device three times with distilled water to establish the gamma flask (γ_f) and its coefficient of variation (COV):
   - (COV = $\frac{\sigma}{\overline{X}}$; standard deviation divided by the mean) where the standard deviation is based on a minimum of three consecutive tests.
   - Recommended maximum acceptable limit for the COV of the gamma flask is 5 percent.
2. Run the device three times with a standard reference material with known COTE (e.g., glass) to establish the correction factor (if needed) for the gamma flask (γ_f) and its COV based on a minimum of three consecutive tests:
   - The correction factor for γ_f is the average of three ratios and is determined from the tests by dividing the γ_f (avg. γ_f through the item 1) and the γ_f to exactly match the COTE of the reference material. Use the 'γ_f' correction factor for all aggregate COTE tests.
   - Recommended maximum limit for the COV of the 'γ_f' correction factor is 5 percent.
   - By fixing the limits for steps 1 and 2, the variability from test to test will be limited to an acceptable range. If the specified COV limits are not met, then repeat the test until the measured COV falls below the required limit.
3. Run the device three times with any aggregate material (e.g., granite) to determine aggregate COTE and its actual COTE COV:
   - Calculated COTE COV is based on the COV of the gamma flask and correction factor for Δh from spreadsheet (described in Appendix C).
   - Assign correction factor (if necessary) for calculated COTE COV in order to match the actual aggregate COTE COV determined from the three tests (this value is expected to be less than 5 percent).

- Use this correction factor to adjust the calculated COTE COV from the spreadsheet for future tests.

Note: Repeat the calibration process every six months. Repeat the calibration process after any changes in the float system/LVDT and any repair work for the dilatometer. Tests of highly porous fine-grained sedimentary rocks (e.g., limestone, sandstone, etc.) must be checked for re-saturation when the aggregate is held at 10°C (50°F) at the beginning of the test and at the end of the test when the sample is held at 50°C (122°F). The Δh used to calculate the COTE for these types of aggregates must reflect the effects of re-saturation.

APPENDIX C

VARIANCE ANALYSIS

$$\gamma_f = \gamma_w - \frac{\Delta h A_t}{V_{f_{10}} \Delta T} - \frac{V_{a_{10}}}{V_{f_{10}}}\gamma_w + \frac{V_{a_{10}}}{V_{f_{10}}}\gamma_a$$

$$\gamma_a = \frac{1}{V_{a_{10}}}\left[\frac{\Delta h A_T}{\Delta_T} + V_{a_{10}}\gamma_w - (\gamma_w - \gamma_f)V_{f_{10}}\right]$$

$$V_{a10} = V_a[1 - \Delta T \gamma_a]$$

$$V_{f10} = V_{w10} + V_{a10}$$

$$Var[\gamma_a] = f(\Delta h V_a \gamma_f \gamma_w) = X_i$$

$$= \sum\left(\frac{\partial \gamma_a}{\partial X_i}\right) VarX_i + \sum\sum \frac{\partial \gamma_u}{\partial X_i}\sigma_i \frac{\partial \gamma_u}{\partial X_i}\rho_{ij}$$

$$VarV_a = \left(\frac{\partial Va}{\partial W}\right)^2 Var(W) = \left(\frac{1}{G\gamma w}\right)^2 \left(Cov(W)\overline{W}\right)^2$$

$$Var\,\gamma_f = (COV(\gamma_f)\overline{\gamma_f})^2$$

$$Var\,\gamma_w = (COV(\gamma_w)\overline{\gamma_w})^2$$

$$Var\,\Delta h = \left(COV(\Delta h)\overline{\Delta h}\right)^2$$

$$Var\ \gamma_a = \left[\frac{1}{V_a}\cdot\frac{A_T}{\Delta T}\right]^2 Var\ \Delta h + VarV_a\left[\frac{\gamma w - \gamma a}{V_a}\right]^2 VarV_a$$

$$+ \left[\frac{V_f}{V_a}\right]^2 Var_f + \left[\frac{1}{V_a}(V_a - V_f)\right]^2 Var\ \gamma_w$$

$$Var\ \gamma_a = \frac{1}{V_a^2}\left[\begin{array}{l}\left(\frac{A_T}{\Delta T}\right)^2 Var(\Delta h) + (\gamma_w - \gamma_a)^2 Var(V_a) \\ + (V_f)^2 Var(V_f) + (V_a - V_f)^2 Var\ \gamma_w\end{array}\right]$$

$$+ \rho(V_{a10})^2\left(\frac{At}{\Delta T}\right)\sqrt{Var\ \Delta h} + (V_{w10} + V_{a10})\sqrt{Var\ \gamma_f}$$

where

V = total inner volume of the flask,

V_w = volume of water in the flask,

V_f = volume of the flask,

V_{a10} = volume of aggregate in the flask,

γ_a = coefficient of volumetric thermal expansion of aggregate,

γ_w = coefficient of volumetric thermal expansion of water,

γ_f = coefficient of volumetric thermal expansion of flask,

A_T = inner sectional area of tower,

Δh = rise of the water surface inside the tower, and

ΔT = temperature increase from T_1 to T_2.

APPENDIX D

GUIDELINES FOR VACUUMING

1. Wash the aggregates thoroughly with distilled water to remove silts, clays, and other fine materials. Select the required quantity of aggregate for the test and immerse in distilled water.
2. Soak the washed aggregates overnight in a container to ensure a high degree of saturation using distilled water.
3. After 24 hours, transfer the aggregates to the dilatometer very carefully after the dilatometer has been half-filled with distilled water to ensure that there is no air trapped between the aggregate particles.
4. After ensuring against possible leakage, for less porous, coarse-grained, hard, and compact aggregates (e.g., hard, compact, and fresh sandstone, granite, some gravel, and marble) and concrete continue vacuuming for the next 60 minutes while checking that the pressure gage needle does not fluctuate and that the mercury level in the cylinder is near zero. Deviation from these conditions suggests possible leakage. An additional period of vacuuming may be required in case of highly porous, fine-grained, weathered sedimentary rocks (e.g., limestone, sandstone, etc.). In case of standard reference materials (e.g., glass, copper, steel, etc.) and water, experience has indicated 45 minutes is sufficient to reduce the air bubble flow to a negligible level.
5. At the completion of each 15 minute vacuuming and vibration period, note the intensity of the flow of air bubbles through the window in the tower before stopping. Intensity may vary from sample to sample but it is recommended to continue the vacuuming until the flow of air bubbles is reduced to a negligible level.
6. During the vacuuming process, it is helpful to apply vibration to the dilatometer. A variable speed Gilson Vibro-Deairator (SGA-5R) was used at TTI. A specific modification adapted the dilatometer to fit on the Vibro-Deairator. Maximum vibration should be applied during the vacuuming process. The effectiveness of the vacuuming de-airing can be monitored by observing the air bubble flow through the window in the tower.

7. Some pores (deep inside) may still remain unsaturated after the vacuum saturation through steps 1-6. These unsaturated pores may come out during expansion due to heating (as a part of the test procedure) and can give erroneous results or variation in results (e.g., high percent COV). To address this issue, an additional research (Appendix F) is conducted and results showed that an additional vacuuming at 50°C along with alternate heating and cooling cycles is very effective to achieve consistent result with permissible variation.

APPENDIX E

SAMPLE PREPARATION

A sampling protocol is introduced to obtain a representative powder sample; following are the steps involved.

1. Thoroughly wash sample to remove foreign materials (i.e., soil, organics, etc.).
2. Visually inspect the samples with a magnifying glass to judge the aggregate heterogeneity. Aggregate consisting of mainly one type of particle with respect to shape, color, and texture is considered to be as homogeneous (e.g., crushed limestone). On the other hand, aggregate with different types of particles with respect to shape, color, grain size, and texture is considered to be heterogeneous (e.g., gravel). Accurate judgment of heterogeneity is necessary for selecting suitable methods in the following steps.
3. Cone and quarter the sample; the number of cycles of cone and quartering depend on amount of sample needed and level of heterogeneity within the sample, as suggested below (for one bag of sample, i.e., 50 lb):
   - 1 cycle for highly heterogeneous samples, e.g., gravel.
   - 2 cycles for intermediate samples, e.g., impure limestone, sandstones, etc.
   - 3 cycles for homogeneous samples, e.g., pure limestone.
4. Dry the selected amount of sample overnight in oven at 60°C.
5. Crush the entire sample using a jaw crusher or similar type of device.
6. Cone and quarter the crushed sample. The number of cycles is determined as follows:

- 3 cycles for highly heterogeneous samples because the selected amount before crushing is high.
- 1 or 2 cycles for homogeneous or less heterogeneous samples.

7. Grind the entire sample using a powdering device (e.g., pestle and mortar for small quantities of sample or ball mill for larger quantities of sample, particularly in the case of highly heterogeneous samples) to pass through a number 200 sieve (75 μm).
8. Analyze powder samples by XRF to determine the bulk chemistry.

APPENDIX F

ADDITIONAL AGGREGATE (Trinity Gravel) COTE TESTING BY DILATOMETRY

Test with different temp. cycle combinations	First Batch of 3029 g of sample (Sp. Gr. 2.695)		Second Batch of 2941 g of sample (Sp. Gr. 2.696)			
	Test 1		**Test 2** (removed the sample of test 1 from the dilatometer and tested a new lot of sample as a 2nd batch)		**Test 3**: Exp. Stopped after Test 2, float removed and put it back and again tested the same sample of test 2	
	Avg. COTE	COV%	Avg. COTE	COV%	Avg. COTE	COV%
Avg. of 3 cycles (2 heating and 1 cooling)	9.56	6.91	9.71	6.92	9.35	6.87
Avg. of 4 cycles (2 heating and 2 cooling)	9.61	5.72	9.75	5.68	9.47	6.11
Avg. of 5 cycles (3 heating and 2 cooling	9.46	6.00	9.52	7.43	9.44	5.34
Avg. of 6 cycles (3 heating and 3 cooling)	NA	NA	9.58	6.77	9.47	4.80
Avg. of 7 cycles (4 heating and 3 cooling)	NA	NA	9.50	6.55	9.37	5.24
Avg. of 3 heating cycles	9.24	7.54	9.08	4.68	9.17	5.31
Avg. of 2 cooling cycles	9.81	0.43	10.17	4.34	9.85	0.17
Avg. of 4 heating cycles	NA	NA	9.08	3.82	9.08	4.93
Avg. of 3 cooling cycles	NA	NA	10.08	3.54	9.76	1.65

- All COTE values are in 10^{-6}/°C, NA – Not Available

Initial and Final water level measurement

- Initial water level position (h_1) – average of collected LVDT readings at stable initial testing temp (10°C) excluding the first 40 minutes and last 15 minutes data (as shown in the figure below)
- Final water level position (h_2) – average of collected LVDT readings at stable final testing temp. (50°C) excluding the first 40 minutes and last 30 minutes data (as shown in the figure below)
- The present initial (at stable 10°C) and final (at stable 50°C) LVDT displacement level calculation (as described in the figure below) is adequate.

- The slope method instead of direct measurement of initial and final level has been applied to calculate the $\Delta H/\Delta T$. The nonlinear relationship (2nd order polynomial) between temperature and displacement (i.e., slope changes with temperature) is the inherent limitation involved in the slope method. However, an attempt has been made to calculate $\Delta H/\Delta T$ by taking derivative of the 2nd order polynomial equation and with a fixed temperature (average of low and high temperatures). However, the results are not consistent.

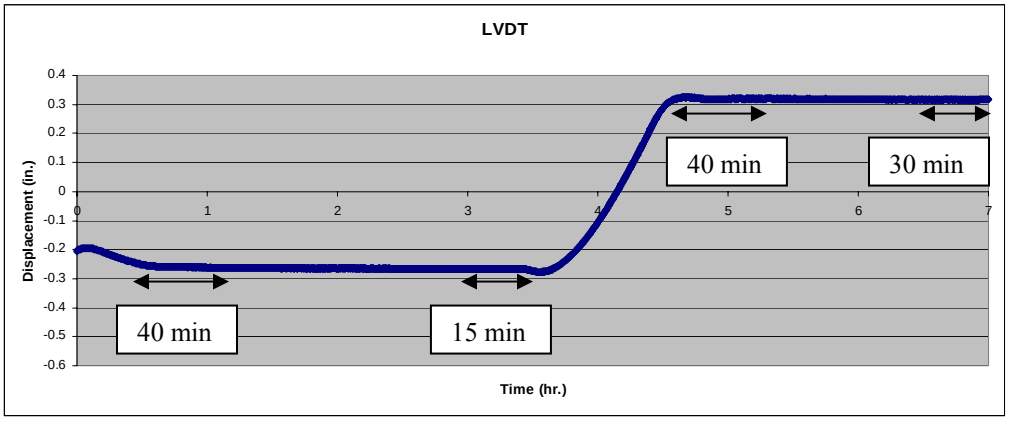

Initial and final water level measurement procedure

Discussion

- The results with varying no. of cycles remain almost the same. The percent COV of all the tests with different cycles varies from 5 to 7.
- Therefore, average COTE of first three cycles (two heating and one cooling) can be representative COTE of the tested samples provided the percent COV of individual test run (e.g., percent COV for the three COTE values corresponding to three cycles in test 1 is 6.91) should be ≤8 percent and percent COV of the average COTE of different test runs should be ≤5 percent . The duration of the three cycles test should be ~ 10.5 hours (1st cycle – 5 hours; 2nd cycle – 2.5 hours; 3rd cycle – 3 hours) as a minimum.
    - percent COV of individual tests, i.e., test 1, test 2, and test 3 are 6.91, 6.92, and 6.87 percent, respectively – these are below the 8 percent limit

- The COTE of the tested gravel = 9.54 (avg. of test 1, 2, and 3) with percent COV = 1.5 percent. Therefore, percent COV of three COTE values from three tests is below the 5 percent limit

Comparison between TTI and TxDOT results

	TTI♣	TxDOT *
COTE (10^{-6}/°C)	9.54%, 1.5%	9.34%, 14%

♣ 2 different samples from the same lot with 3 heating cycles (test 1, 2 and 3 mentioned above) and additional vacuuming at 50°C

* 3 different samples from the same lot with one heating cycle (10°-50°C) and no vacuuming at 50°C

Note – Application of additional vacuuming at 50°C and temperature cycles (as in TTI testing) improves the percent COV.

APPENDIX G

ITEM 421 SPECIAL PROVISION: COTE TESTING

421.2. Materials.

E. Aggregate.

1. Coarse aggregate. *Coefficient of thermal expansion (COTE) of coarse aggregate shall not exceed the values specified by engineer when tested in accordance with Test Method Tex-xxx. The Test method Tex-xxx is based on two approaches, i.e., direct measurement by Dilatometer (Tex-xxx-A) and prediction by mineralogical modeling (indirect, Tex-xxx-B)). The sampling of coarse aggregate for COTE measurement shall be done in accordance with test method Tex-yyy. COTE of one coarse aggregate sample per 2000 ton of aggregate use shall be tested in accordance with Test Method Tex-xxx-B and COTE of one coarse aggregate sample per 12,500 ton of aggregate use shall be tested in accordance with Test Method Tex-xxx-A.*

421.9. Quality of concrete. *Concrete COTE shall be predicted in accordance with the Test Method Tex-xxx-C where determined COTE of coarse aggregate and standard mortar by Test Method Tex-xxx and volume fractions of coarse aggregate and mortar from mixture proportions are the primary inputs. If the sand is other than the conventional silica sand then mortar COTE in Test Method Tex-xxx-C shall be adjusted. The predicted concrete COTE in accordance with the Test Method Tex-xxx-C shall conform to the specified range for specific project. Any deviation of concrete COTE shall be adjusted by slight change of mixture proportion within acceptable limit.*